MODELLING AND PERFORMANCE EVALUATION OF A SOOT CYCLONE SEPARATOR

by

L.D.J. Bieldt

12987654

Mini-dissertation submitted in partial fulfilment of the requirements for the degree

Master of Nuclear Engineering

at the Potchefstroom Campus of the North-West University

Supervisor: Prof. P.G. Rousseau

Co-supervisor: Mr J. Holtzhausen

March 2009

Approved by _____
Chairperson of Supervisory Committee

_____

Programme authorised
to offer qualification _____

Date _____

NORTH-WEST UNIVERSITY

ABSTRACT

MODELLING AND PERFORMANCE EVALUATION OF A SOOT CYCLONE SEPARATOR

by L.D.J. Bieldt

This mini-dissertation reports on the performance of a cyclone separator used to remove excess soot that is typically formed during the production of pebble fuel for High Temperature Gas-cooled Reactors.

A chemical vapour deposition process is used to manufacture TRISO-coated fuel particles and during this process soot is formed that needs to be removed. This removal process uses cyclone separators as pre-filters and a bag filter as the final means of preventing unwanted particles from being introduced into the atmosphere. An important requirement of the cyclone separator is the need for a safe geometry design. This implies that the containment of enriched-uranium fuel particles can under no circumstances result in a criticality situation. An advantage of this safe geometry design is that it eliminates the use of expensive gamma detectors within the cyclone separator. In this min-dissertation, the performance of a new safe geometry cyclone separator design to be used in the removal of soot in the manufacturing of TRISO-coated particles was investigated via theoretical modelling.

Various models for predicting the performance of cyclone separators are in existence. These were examined and the best-suited model for the task at hand was selected. The model as described by Li and Wang appeared to be the most applicable and useful, given the available information, such as the cyclone geometries and particle characteristics. Li and Wang's model, as with many of the other models in the literature, were developed to calculate the collection efficiency. This model was first benchmarked with empirical data obtained from the current cyclone separator used in the production of coated particles at the Pebble Bed Modular Reactor (PBMR) Advance Coater Facility (ACF) situated at Pelindaba in South Africa.

The calibrated model was then used to predict the collection efficiencies of three newly designed cyclone separators. The results obtained from the model predicted an increase in collection efficiency for all the newly designed cyclone separators when compared to the existing units. Therefore, this project found that any of the newly designed cyclones should serve as a good alternative to the current cyclone separator.

NOORDWES-UNIVERSITEIT

OPSOMMING

MODELLERING EN PRESTASIE EVALUASIE VAN 'n ROETSIKLOONSKEIER

deur L.D.J. Bieldt

Die werkverrigting van 'n roetsikloonskeier word in hierdie skripsie opgeteken. Die sikloonskeiers word tipies gebruik tydens die vervaardiging van korrelbedbrandstof vir Hoë Temperatuur Gasverkoelde Reaktors om ongewenste roet te verwyder.

Die TRISO-bedekte brandstof partikels word vervaardig deur 'n chemiese damp-neerslag proses en tydens die proses word die roet gevorm wat verwyder moet word. Die verwyderingsproses word uitgevoer deur sikloonskeiers te gebruik as voor-filters en sak filters word as die laaste metode van skeiding gebruik om te verhoed dat die ongewensde partikels vrygelaat word in die atmosfeer. Een belangrike vereiste van die sikloonskeier-ontwerp is dat dit uit 'n veilige geometrie moet bestaan. Dit impliseer dat die houer (sikloonskeier) van die verrykte uraan brandstof partikels onder geen omstandighede kritikaliteit sal bereik nie. 'n Voordeel van veilige geometrie-ontwerp is die uitskakeling van duur gamma sensors wat nodig is om reaktiwiteit te toets binne die sikloonskeier. Dus moet die prestasie van hierdie nuwe sikloonskeier-ontwerp, wat gebruik word tydens die vervaardiging van TRISO-bedekte partikels, in hierdie navorsingsprojek voorspel word deur middel van teoretiese modellering.

Verskeie bestaande modelle wat gebruik word om die prestasie van 'n sikloonskeier te modelleer was ondersoek en die mees toepaslike model was gekies. Die model soos beskryf deur Li en Wang het as die mees gepaste model voorgekom, as die beskikbare informasie in ag geneem word, byvoorbeeld sikloon geometrie en partikel karakteristieke. Li en Wang se model, soos baie van die ander modelle in die literatuur, word gebruik om die kollektiewe effektiwiteit van 'n sikloonskeier te bereken. Die model was eers gemaatstaf met empiriese data ontvang van die huidige sikloonskeier wat gebruik word om die bedekte partikels te vervaardig vir *Pebble Bed Modular Reactor* (PBMR) by die *Advance Coater* fasiliteit by Pelindaba in Suid-Afrika.

Die gekalibreerde model was toe gebruik om die kollektiewe effektiwiteit te voorspel van die drie nuut-ontwerpte sikloonskeiers. Die resultate het getoon dat die effektiwiteit van die nuwe ontwerpe beter is as die huidige sikloonskeier-ontwerp. Dus het hierdie projek gevind dat enige een van die drie sikloonskeiers 'n goeie alternatief bied vir die huidige sikloonskeier.

TABLE OF CONTENTS

LIST OF FIGURES

LIST OF TABLES

ACKNOWLEDGEMENTS

The author wishes to express sincere appreciation towards Prof. Rousseau and Mr Jacques Holtzhausen for their assistance with this research project and preparation of this mini-dissertation. In addition, special thanks go to Mr Johan Markgraaff (Jnr.) and his team at M-Tech Industrial (Pty) Ltd, whose familiarity with the coater facility and design requirements was helpful during the early programming phase of this undertaking. The author offers great appreciation towards Sabrina Raaff for her exceptional reviewing work on this mini-dissertation.

The author thanks his family and all his friends for their personal backing during the entire duration of this mini-dissertation, especially Henna.

Soli Deo Gloria.

GLOSSARY

ACF	Advance Coater Facility
BC	Black carbon
CFD	Computational Fluid Dynamics
CS	Cyclone separator
CVD	Chemical vapour deposition
EES	Engineering Equation Solver
FP	Fission product
GUI	Graphical user interface
HTGR	High Temperature (Gas-cooled) Reactor
ISO	International Organization for Standardization
PAH	Polycyclic Aromatic Hydrocarbon
PBMR	Pebble Bed Modular Reactor
PFP	Pilot Fuel Plant (situated in South-Africa)
PM	Particulate matter
PoC	Post cyclone
PSD	Particle size distribution
PyC	Pyrolytic carbon
SEM	Scanning electron microscope
SiC	Silicon carbide
SG	Safe geometry
SPL	Sound pressure level
TEM	Transmission electron microscopy
TRISO	Tristructural isotropic

CHAPTER 1: INTRODUCTION

1.1 Motivation

The world's population is an ever-demanding energy consumer and solutions are required to meet growing energy needs. Power sources with carbon-free emissions are increasingly popular; thus nuclear power generation is receiving increased attention, even though it was viable long before carbon emissions were considered a problem. High Temperature Gas-cooled Reactor (HTGR) fuel manufacturing is very important because better fuel quality ensures improved fission product (FP) retention at higher temperatures. This increases the safety and economy of the reactor. Soot is produced in the current fuel manufacturing process and, if not controlled, poses environmental and health risks.

Researchers are urging regulators and the authorities to revise the regulatory acts that monitor and regulate smoke emissions. Science Daily (2009) states that soot emissions pollute not only the surrounding area, but also the downwind areas. Soot travels great distances; therefore, it is of concern that it darkens ice surfaces (at the poles and on mountain peaks), which absorbs sunlight better and melts quicker thus contributing to global warming. Swaney (2007) estimates that 50 000 Americans die prematurely from particle-related exposure. Tsai *et al*. (2001) demonstrate that there are health risks involved in the inhalation of polycyclic aromatic hydrocarbons (PAHs). These small particles can easily be inhaled and are trapped inside the lungs. Therefore, unwanted emissions should be removed before the gas can be released into the atmosphere. This is even more important in the case of the soot under consideration here.

1.2 Background

At the Pilot Fuel Plant (PFP) in South Africa, fuel is manufactured for the Pebble Bed Modular Reactor (PBMR). At this plant, TRISO-coated (tristructural isotropic) particles are manufactured for use in the reactor at the division called the Advance Coater Facility (ACF). These particles form the basis of the inherent safety of the reactor. The coated particle consists of a uranium dioxide kernel with a diameter of between 200 µm and 600 µm that has an inner porous graphitic buffer layer. The buffer layer is then coated with three additional layers, namely inner pyrolytic carbon (PyC), silicon carbide (SiC) and another outer pyrolytic carbon layer as seen in Figure 1. The inner porous layer or

buffer layer captures many of the fission products (FPs) formed during fissions in the kernel. The buffer layer is porous and contains small internal voids to prevent the kernels from swelling during high burn-up (high usage). The main function of the inner and outer PyC layers is to physically protect the very dense SiC layer. The SiC layer is the main barrier against FP migration and mechanical shock. During the manufacturing of the TRISO-coated particles unwanted soot is generated, which is fed into an off-gas system where the soot is then removed before the gas is released into the atmosphere (NWU, 2009:2–26).

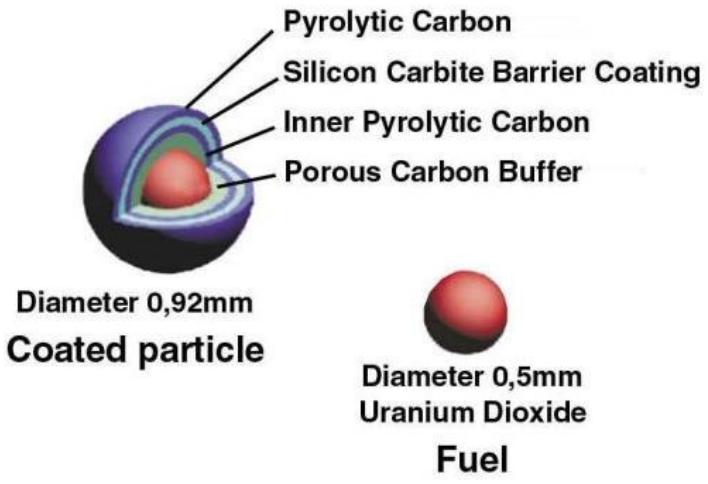

Figure 1: TRISO-coated particle

1.3 Problem statement

As mentioned above, during the manufacturing of TRISO-coated particles at the PFP unwanted soot is formed. The current plant design makes use of cyclone separators (CS) to remove much of the soot before the final filter removes the remaining particles. The final stage uses a bag filter that needs to be cleaned frequently. There is a need to design a pre-filter to reduce the frequency at which the bag filter is cleaned. The pre-filter should not unduly disturb the flow of the fuel manufacturing cycle, in order for the process to be as similar as possible to the original German manufacturing method. This method has already been accepted as proven technology and thus needs to be replicated as close as possible.

The new cyclone should have safe geometry (SG). This means that a criticality situation will not arise even if the CS is full of uranium kernels. A sustainable nuclear chain reaction, termed *criticality*, can occur if the following conditions are satisfied: suitable geometry and correct mass and temperature of fissionable material. The geometry of a CS can be designed to prevent criticality. This SG design eliminates the need for expensive gamma sensors to detect criticality inside the CS. The current CS does not have SG and various new SG designs were done and provided for evaluation of collection efficiency in this study. There is a need to use a simple model to predict the collection efficiencies of these new designs. If the new cyclone designs achieve the same collection efficiency as the current design, it will be regarded as an improvement as they will have safe geometry designs.

1.4 Research objectives

The following objectives will be addressed:

1. Detailed literature study on CS performance
2. Justify an appropriate theoretical model to predict CS performance
3. Report on the theoretical predictions of the new CS designs
4. Establish if the proposed CS's will be a good alternative to the current design

1.5 Chapter outline

A literature study was conducted on soot agglomeration with a focus on solid-gas CS's and collection efficiency models of these CS. After a comprehensive literature study a suited model was chosen and programmed. Experimental data was supplied by the PBMR from the ACF. This data was used to validate a theoretical model that was used to predict the collection efficiency of the new CS designs that can be used in the ACF. This validation process will be captured within the Modelling Methodology chapter. The results were calculated and then documented. These results will indicate whether the theoretical model is applicable for future predictions. Thus conclusions were derived from these theoretical results, regarding the best CS design with the advantages and disadvantages of each CS. Recommendations was made in the final chapter to enhance future development and address the concerns of CS design and modelling. This chapter outline is graphically depicted in Figure 2 below.

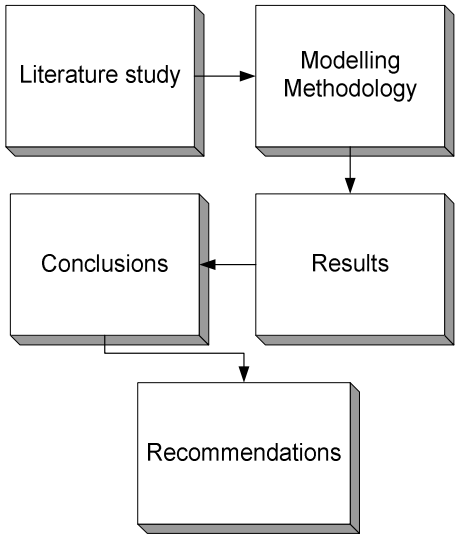

Figure 2: Chapter outline

1.6 Chapter summary

This chapter has provided the project's motivation, problem statement and objectives. The chapter has also outlined the chapters that follow in this mini-dissertation. The mini-dissertation reports on a proposed solution that can enhance the safety and cost of soot removal during the TRISO-coated particle manufacturing process. The literature study that follows this chapter will give an in-depth discussion of the project terminology and functionality.

CHAPTER 2: LITERATURE STUDY

2.1 Pilot Fuel Plant

Through a variety of processes, the PFP manufactures the fuel pebbles used in the PBMR. The ACF forms part of the larger process. A simplified flow diagram of the ACF is presented in Figure 3. The chemical vapour deposition (CVD) process is a technique that uses different gases to produce the different layers of the TRISO-coated particles as shown in Figure 1 (the CVD process is explained in Section 2.2). The gases exit at a very high temperature and enter a heat exchanger that cools them. The gases are transported by a blower at the end of the cycle and move through the CSs 1 and 2 in Figure 3. The first cyclone (CS1) is 60.2% efficient, while the second (CS2) is 15% efficient. The remaining soot is removed by the bag filter where the soot-free gases are then released into the atmosphere.

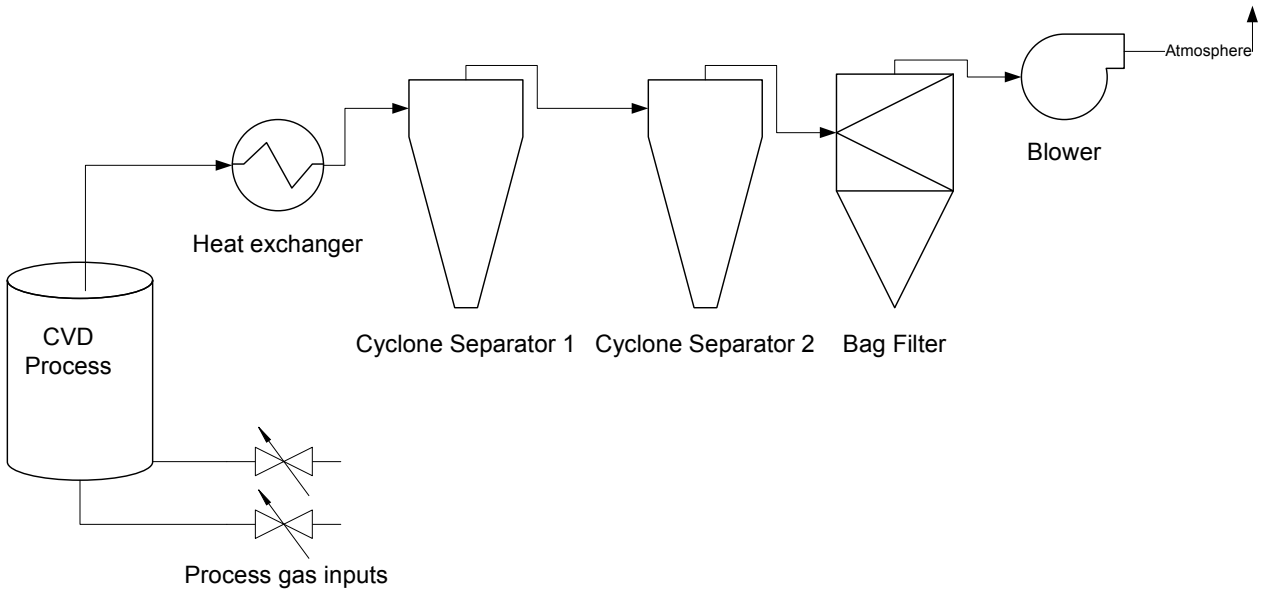

Figure 3: Advanced Coater Facility basic flow diagram

2.2 Chemical vapour deposition

From Figure 1, it can be seen that the red sphere represents the uranium dioxide fuel kernel (in actuality it is black with a diameter of approximately 500 µm) with four concentric layers formed around it. Each layer has a specific function to ensure good quality fuel. These four layers are typically manufactured using a fluidised bed CVD coater. The coater has a cylindrical geometry and a mixture of different gases enters the bottom of the coater. The whole process is carried out at approximately 1600°C, which forces the different gases to decompose. The different stages of coating each layer entail the following gases (Uner, 2007:9; Nothnagel & Venter, 2006:27, 35):

- buffer layer: decomposition of acetylene (C_2H_2) using Argon as a carrier gas;
- inner pyrolytic carbon layer: decomposition of propylene (C_3H_6) using Argon as a carrier gas;
- silicon carbide layer: decomposition of methyltrichlorosilane (CH_3SiCl_3) using Hydrogen as a carrier gas; and
- outer pyrolytic carbon layer: decomposition of C_3H_6 using Argon as a carrier gas.

Each layer has its own typical parameters that are dependant on a specific pressure, temperature, gas mixture and flow rate. Unwanted soot is formed during decomposition of these gases. It was observed that if both the temperature and the concentration of the gases were increased, more soot was found on the top of the CVD coater (López-Honorato *et al*., 2008:3122–3123). Furthermore, it was noted that if either the temperature or concentration of gases was lowered there were fewer polycyclic aromatic hydrocarbons (PAH) and less soot, owing to lower gas phase maturation (López-Honorato *et al*., 2009:407; soot and PAHs are discussed in more detail in Section 2.6).

2.3 Cyclone separators

Cyclone separators are popular systems by which solids may be removed from a medium such as liquid or gas. A CS that removes solids from a liquid is commonly known as a hydro-cyclone. This project focused on CSs that remove solids from a gas, which are termed *gas-solid cyclones*. A cyclone is constructed with stationary parts that rotate the inlet gas containing the solids. The geometry of a CS is such that the gas forms a vortex that removes particles through centrifugal force. Owing to this relatively simple design, cyclones are inexpensive to build and mechanically simple with

low maintenance. A shortcoming of CSs is relatively low collection efficiency when they are used to remove particles smaller than 5 μm in diameter or particles with a low mass density. Cyclones can be designed to operate in various conditions, such as high/low temperatures, high/low inlet velocities and high/low flow rates, and from small to industrial scale capacities. These features allow cyclones to be used in a wide range of applications.

Cyclones have been used since the 1880s to remove solids from gases, but the first published efforts of cyclone performance was documented only in the 1930s. In the 1940s, extensive effort was focused on the flow patterns of the gas inside a cyclone, which led to many theories predicting the pressure drop and collection efficiencies of different cyclones. Well-known theories used for cyclone performance include *Alexander*, *Barth, Shepherd* and *Lapple*, *Stairmand* and *First* (Fayed & Otten,, 1984:730–733).

2.3.1 Cyclone separator design

The most common design for a CS is termed the *reverse-flow* or *cone-under-cylinder design*, as is shown in Figure 4. The straight-through design works on the same principal as the reverse-flow design but uses swirl vane entries to rotate the gas. However, these straight-through designs are rarely used in industry and little data is available on them.

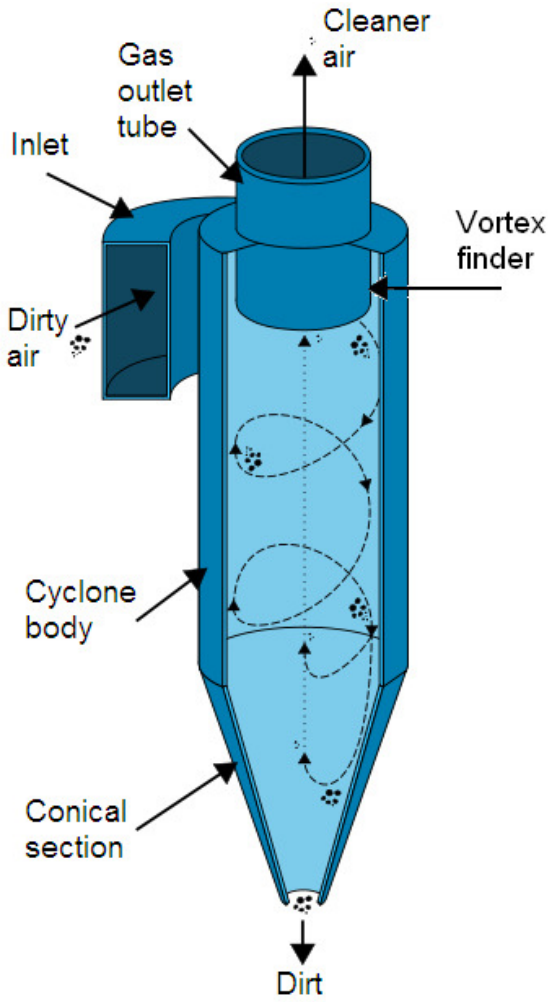

Figure 4: Cyclone separator
(http://en.wikipedia.org/wiki/Cyclonic_separation)

There are standard geometries for different CS designs and these geometries can be expressed in different dimension ratios relative to the diameter D_c of the cyclone. These ratios can be used to design a cyclone for required throughput or efficiency. Table 1 below provides general and standard ratios typically found in CSs, which were obtained from Fayed and Otten (1984:733). In conjunction with Table 1, Figure 5 demonstrates basic measurements used to describe a CS. Note that distance *S* depicts the so-called vortex finder length, and diameter B_c can be connected to what is termed a *dipleg*. A dipleg connects the bottom of a cyclone (dust outlet) to a collection bin (hopper). See Figure 12 for a visual display of a dipleg.

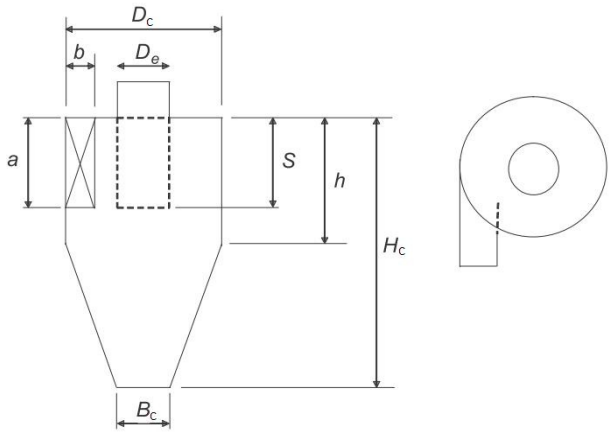

Figure 5: Cyclone dimensions

Table 1: Standard designs for reverse-flow cyclones (Fayed and Otten, 1984)

Source	Stairmand	Swift	Lapple	Swift	Stairmand	Swift
Recommended duty	**High efficiency**	**High efficiency**	**General purpose**	**General purpose**	**High throughput**	**High throughput**
D_c	1.0	1.0	1.0	1.0	1.0	1.0
a/D_c	0.5	0.44	0.5	0.5	0.75	0.8
b/D_c	0.2	0.21	0.25	0.25	0.375	0.35
D_e/D_c	0.5	0.4	0.5	0.5	0.75	0.75
S/D_c	0.5	0.5	0.625	0.6	0.875	0.85
h/D_c	1.5	1.4	2.0	1.75	1.5	1.7
H_c/D_c	4.0	3.9	4.0	3.75	4.0	3.7
B_c/D_c	0.375	0.4	0.25	0.4	0.375	0.4

From Table 1, it can be seen that the higher efficiency CS has a smaller inlet ratio (a/D_c, b/D_c) and smaller gas outlet ratio (D_e/D_c) than the high throughput cyclones. A CS should be designed to fulfil a particular function. This function depends on the need of the applications for which the CS will be used, which will pose specific requirements regarding collection efficiency, pressure drop, throughput and/or the number of cyclones.

2.3.2 Cyclone separator performance modelling

Modelling the performance of a CS entails more than calculating the collection efficiency or the amount of solids removed in a gas-solid CS. Developed theories predict the pressure drop, the internal gas flow patterns, pressure distributions and even the solid concentration of different size particles in a CS. Many of the alternative models currently available are used to enhance the collection efficiency models but require excessive computation, computational fluid dynamics (CFD) modelling and a variety of data inputs, for example friction factors, drag coefficients of particles and flow patterns inside the cyclones.

In Figure 6, the white colour represents the particles' position within a CS and the black colour depicts no particles. Therefore, it can be seen that the particle size has an effect on predicted particle position inside the CS. Wan *et al*. (2008:97) simulated particles of different sizes and note that the particles with smaller diameter accumulate at the top of the cyclone, and that by increasing the diameter of the particles the accumulation height (the height above the hopper) decreases as seen in Figure 6 (b). It is noted that the smaller particles will escape through the vortex finder. Improvements can be made on the collection efficiency by using models such as these by, for example, either enlarging the particles (agglomeration techniques) or changing the geometry of the vortex finder.

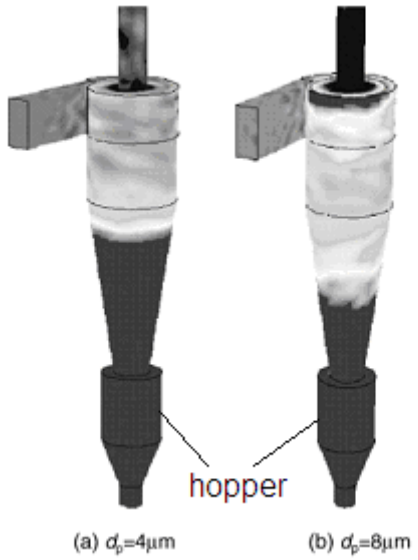

Figure 6: Particle concentration on the walls (Wan *et al*., 2008)

2.3.3 Collection efficiency theory

Collection efficiency η is defined as the percentage of the incoming particles of a certain size collected by the CS (Fayed & Otten, 1984:738). In principle, there are two movements competing against each other: firstly, the gas-flow movement entering the cyclone moving in a spiral motion downwards; and secondly, the centrifugal force moving outwards towards the wall of the cyclone. The greater this second force is, the more efficient the cyclone will be. The goal is for the particle to hit the wall of the cyclone before it reaches the vortex core that will remove the particle from the cyclone. A brief explanation of Lapple's and Licht's models to calculate the collection efficiency yields an improved understanding of the parameters that affects the CS.

Lapple's model is a basic model that assumes laminar flow. According to Avci and Karagoz (2003:945), laminar flow is assumed when the Reynolds number is below 2300. Lappel's model first calculates the particle diameter (assuming spherical particles) $d_{p50\%}$ that will have 50% collection efficiency under specific conditions. Thus, if $d_{p50\%}$ equals 4 µm for a specific CS, the specific CS will achieve 50% efficiency if all the particles are the size of 4 µm. Equation (2.3.3.1) calculates $d_{p50\%}$, where μ is the viscosity of the gas, b is the inlet width, N_e denotes the number of effective turns the gas makes within the cyclone (usually empirically measured), V_i is the inlet velocity of the gas and ρ_p is the particle density (Fayed & Otten, 1984:742; Wu *et al.*, 2007).

$$d_{p50\%} = \sqrt{\frac{9\mu b}{2\pi N_e V_i \rho_p}} \qquad (2.3.3.1)$$

It is evident from equation (2.3.3.2) below, that the smaller $d_{p50\%}$, the better the collection efficiency. The fraction efficiency η_j represents the collection efficiency of a specific-sized particle. Thus, the fraction efficiency η_j is used to calculate the grade efficiency curves for any other particle size d_{pj} from equation (2.3.3.2). These calculations deliver what is termed the *grade efficiency curves* for a specific cyclone. Examples of these curves are given in Figure 7 and Figure 8 in Section 2.3.4. The grade efficiency curves together with the particle size distribution (PSD), see Section 3.2.3, are used to calculate the total collection efficiency of a CS. Therefore, the calculated grade efficiency curves can remain constant for a specific CS at specific operating conditions but the collection efficiency can

change due to a change in the PSD. For example, the same CS will have different collection efficiencies at the same operating conditions when different types of particles for instance sand or saw dust are introduced into the CS.

$$\eta_j = \frac{1}{1+(d_{p50\%}/d_{pj})^2} \qquad (2.3.3.2)$$

Licht's model is more complex than Lapple's model and assumes turbulent flow. According to Avci and Karagoz (2003:945), turbulent flow is assumed when the Reynolds number is above 3000. As with Lapple's model, Licht's model calculates the 50% collection efficiency for a specific particle diameter given by:

$$d_{p50\%} = \left(\frac{0.693}{A}\right)^{n+1} \qquad (2.3.3.3)$$

where *n* is the vortex exponent that can be calculated (dependant on cyclone diameter and gas temperature) or read off charts (Santana *et al.*, 2001:3; Fayed & Otten, 1984:742; Wu *et al.*, 2007). *A* represents the factor in equation (2.3.3.3) that is calculated by:

$$A = 2\left[\frac{KQ\rho_p(n+1)}{18\mu D_c^3}\right]^{1/2(n+1)} \qquad (2.3.3.4)$$

where *Q* is the gas flow rate, *K* is the configuration factor (dependant on the cyclone geometry) and D_c is the cyclone diameter (see Figure 5). The fractional efficiency is then given by:

$$\eta_j = 1-\exp\left[-0.693\left(\frac{d_{pj}}{d_{p50\%}}\right)^{\frac{1}{n+1}}\right] \qquad (2.3.3.5)$$

In designing cyclones, a basic understanding of which parameters influence collection efficiency is essential. By using basic models such as Lapple's or Licht's models, the designer can comprehend the effect that different changes will have on the performance. From equations (2.3.3.1) and (2.3.3.2), it can be seen that the higher the inlet velocity, particle density or the number of effective turns are, the higher the collection efficiency will be. If the viscosity of the gas is low (see Section 2.4.1 for more detail) and enters a narrow inlet, efficiency will be increased. From equation (2.3.3.4), it is clear that

the geometry of a cyclone also plays an important role. These equations can show the effects of different operating conditions, such as temperature, on collection efficiency, as well as the effects of the various physical dimensions of a CS. The influence of temperature, viscosity, inlet speed, particle concentration and cyclone geometry are discussed in the following sections.

2.3.4 Comparison of various collection efficiency models

Gimbun *et al*. (2004:42) summarise various collection efficiency models and compares them to data obtained by Ray *et al*. (2000:570), and Kim and Lee (1990:1007). These comparisons are given in Figure 7 and Figure 8, respectively. The diamonds in both figures represent empirical data, while the solid lines represent theoretical data. Gimun *et al*. conclude that Li and Wang's model (1989; see Section 3.2.3) performed best to predict these collection efficiencies under ambient conditions. They further improved the Li and Wang model using a modified vortex exponent, which is discussed in Section 3.3.3. Note that the collection efficiency models calculate a grade efficiency curve, as seen in the figures below, these curves are used to calculate the collection efficiency from a specific PSD.

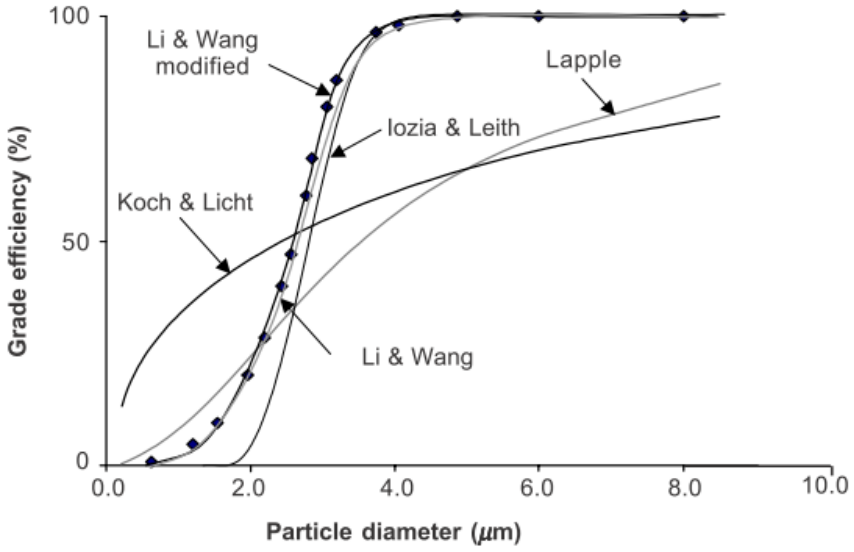

Figure 7: Grade efficiencies (Ray *et al*., 2000)

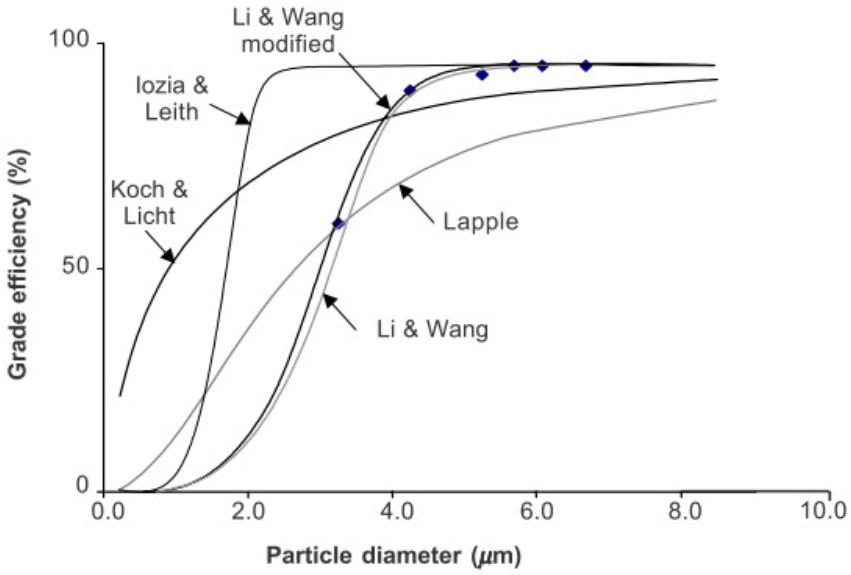

Figure 8: Grade efficiencies (Kim & Lee,1990)

Table 2: Comparison between data

	Ray *et al.* (2000) data	Kim and Lee (1990) data
Temperature (*T*)	293 K	293 K
Inlet speed (v_i)	11 m/s	4.25 m/s
Particle density (ρ_p)	2800 kg/m³	980 kg/m³
Cyclone body diameter(D_c)	0.4 m	0.0311 m

From Table 2, it is evident that the data range is quite broad. The two sets of data differ from low to high inlet speed and light to heavy particle densities and the cyclones that were used had small and large diameters. This wide range of data implies an increased confidence in the models' accuracy and versatility.

2.3.5 Pressure drop calculation

Dirgo (1988; quoted by Ramachandran *et al.*, 1991) derived a correlation between cyclone geometry and pressure drop. Dirgo's pressure drop model (quoted in Ramachandran *et al.*, 1991:136–140) is given as:

$$\Delta P = \Delta H \frac{v_i^{\,2} \rho_G}{2} \qquad (2.3.5.1)$$

where ΔP is the pressure drop in pascal [$kg/(m.s^2)$], v_i is the gas inlet velocity and ρ_G is the gas density. ΔH is defined as:

$$\Delta H = 20\left(\frac{ab}{D_e^2}\right)\left[\frac{S/D_c}{(H_c/D_c)(h/D_c)(B_c/D_c)}\right]^{\frac{1}{3}} \qquad (2.3.5.2)$$

All of the cyclone's physical dimensions are represented in equation (2.3.5.2). This results in a dimensionless parameter that is used to calculate pressure drop from equation (2.3.5.1). Equation (2.3.5.2) was used by Ramachandran *et al.* (1991:140) to predict ΔH for 98 cyclones with relatively good accuracy. Figure 9 depicts the measured ΔH with the circles and the calculated ΔH from equation (2.3.5.2) is represented by the solid line.

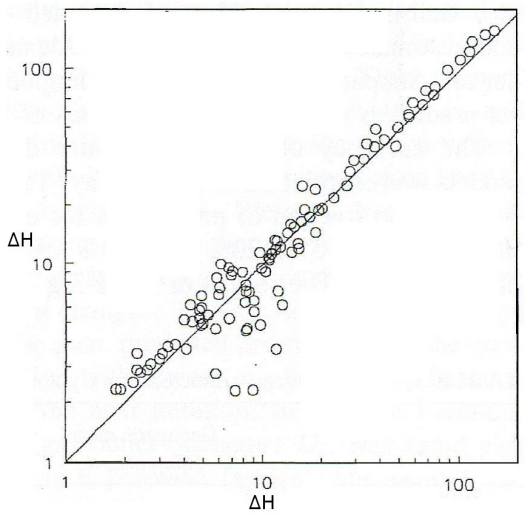

Figure 9: ΔH from equation (2.3.5.2) and observation

2.4 Parameters that influence cyclone efficiency

As mentioned in Section 2.3.3, there are different parameters that have an effect on the CS performance. This section discusses the effects of temperature, viscosity, inlet speed, particle concentration and cyclone geometry. The cyclone geometry includes the following variables: CS inlet and outlet size, body diameter and height, or the dipleg length. This section also discusses the effects that different inlet designs and different inlet entry angles will have on the performance of a CS.

2.4.1 Temperature and viscosity

It was observed by Bohnet (1995:155) that high temperatures have a negative effect on the cyclone total collection efficiency. An experimental cyclone was used to simulate the collection efficiencies at different inlet speeds and increasing temperatures. According to Sutherland's formula:

$$\mu = \mu_0 \frac{T_0 + C}{T + C}\left(\frac{T}{T_0}\right)^{3/2} \qquad (2.4.1.1)$$

where μ is the dynamic viscosity; μ_0 is the reference viscosity; T and T_0 are the input temperature and reference temperature in Kelvin, respectively; and C is the Sutherland's constant. It is evident that the viscosity of gas increases with an increase in input temperature. This has a direct impact on the cyclone efficiency, owing to the higher gas viscosity as previously mentioned (see equation 2.3.3.1 and equation 2.3.3.2).

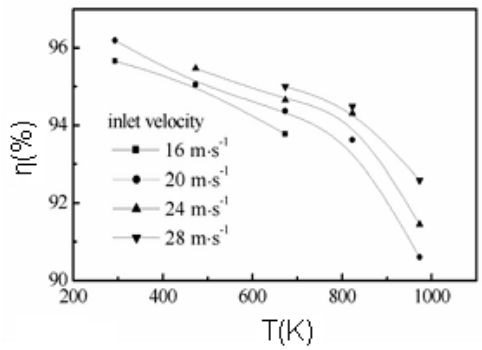

Figure 10: Temperature effect on cyclone efficiency (Chen & Shi, 2003:22)

As can be seen in Figure 10, collection efficiency declines for every inlet velocity with an increase in temperature (Chen & Shi, 2003:22). Even though the gas density decreases with an increase in temperature, this effect is negligible because the relative relation between the densities of the gas and the particles is the contributing influence. A steep drop can be observed above the 800 K range, which is due to a lower vortex component as a result of lower tangential velocity. Chen and Shi (2003:23) note that to some extent higher temperatures allow the submicron particles to agglomerate better because of an increase in the kinetic energy of the gas particles. This will increase the collection efficiency for submicron particles. However, Chen and Shi also note that viscosity plays a greater role at high temperatures than agglomeration owing to the high temperatures; therefore, efficiency drops with higher temperatures.

2.4.2 Cyclone inlet speed

Investigation of empirical data from different experiments (Zhao *et al*., 2004:145; Santana *et al*., 2001:7–8; Xiang *et al*., 2001:553) leads to the conclusion that a higher inlet speed increases collection efficiency (see Figure 10). The reason for this observation is that as the flow rate increases, the inlet speed increases and as a result the centrifugal force applied to the particles also increases. Therefore, the particles will move more rapidly to the side of the cyclone, reducing the likelihood of leaving the cyclone uncollected. As can be seen from equation (2.3.3.1), the greater the inlet velocity and the narrower the inlet width are, the smaller the 50% cut-off diameter will be (the better the efficiency). The same applies to Licht's model, for which it was shown that if the flow rate is increased, and the inlet velocity is thus increased, the efficiency is increased.

2.4.3 Particle concentration

The inlet particle concentration, can be measured as milligram solids per cubic meter of gas (mg/m^3), plays an important part in the total collection efficiency of a CS. The effect of higher particle concentration will result in lower swirl intensity, due to the particles constricting the gas flow to some extent. This was thought to reduce the overall collection efficiency due to lower centrifugal force, but experiments by Ji *et al*. (2009:256) showed the contrary. They found that if a fixed particle size distribution (PSD) is fed into a CS at different concentrations, the total collection efficiencies varied. The results can be seen on the left-hand side of Figure 11: the higher the particle concentration was, the higher the collection efficiencies were. The grade efficiency curves changed marginally with an increase in particle concentration, while the total efficiency increased much more than expected. This

phenomenon was due to an increase in particle agglomeration inside the CS when higher particle concentrations were present. The agglomeration phenomenon is discussed in more detail in Section 2.6.2. However, for improved understanding, the following is to be noted: there is an increase in the inter-particle force (van der Waals forces) when higher concentrations of particles are present because of a shorter distance between the particles (parameter *a* in equation (2.6.2.3)). Particles that have a lower density will have a greater agglomerating effect at higher particle concentrations.

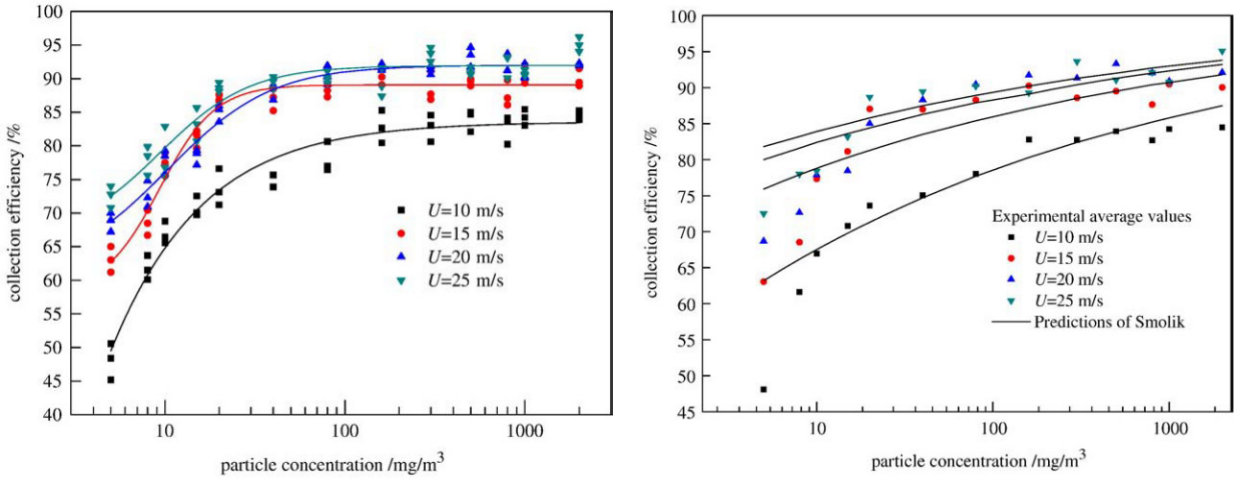

Figure 11: Total collection efficiency versus particle concentration (Ji *et al.*, 2009)

As seen on the left-hand side of Figure 11, the particle concentration has a more prominent effect with lower inlet velocities and higher temperatures (Ji *et al.*, 2009:254). Smolik's model, an empirical model, predicts the total collection efficiency, taking the effect of agglomeration into account, using the following equation from Fayed and Otten (1984:744) and Ji *et al.* (2009:256):

$$\eta(C_2) = 1 - [1 - \eta(C_1)]\left(\frac{C_1}{C_2}\right)^{0.182} \qquad (2.4.3.1)$$

The collection efficiency at $\eta(C_1)$ is known for a specific concentration C_1, from which $\eta(C_2)$ can be calculated as the new collection efficiency for any given particle concentration C_2. Smolik's predictions are shown on the right-hand side of Figure 11. Based on these predictions, Ji *et al.* (2009:259) recommend using Smolik's model for particle concentrations higher than 40 mg/m³. Ji *et*

al. (2009:259) and Cortés and Gil (2007:228) state that collection efficiency models such as Barth, Leith and Licht, and Mothes and Loffer work well at particle concentrations lower than 5 to 10 g/m^3. The soot agglomeration within the CS is still unknown. Therefore, Smolik's prediction was validated from experimental data for this research project.

2.4.4 Cyclone geometry

Apart from particle concentration and temperatures that have an influence on cyclone efficiency, the geometry of a cyclone also plays an important role. Licht's model has two parameters that are dependant on the cyclone's geometry. Equation (2.3.3.4) gives the vortex exponent *n* and the configuration factor *K*. The higher both these components are, the more efficient the cyclone will be. However, the experimental results from Xiang *et al*. (2001:557–558) contradict these assumptions. Thus, there is a need to examine empirical studies in order to determine which geometric dimensions can have a positive influence on collection efficiency.

Avci and Karagoz (2003:952–953) conclude the following regarding the dimensional changes in cyclones: large cyclones are usually fully turbulent while smaller cyclones or low flow rates can cause laminar flow. They also note that if the height of the cyclone (H_c in Figure 5) is increased while keeping the other dimensions constant, the collection efficiency will be positively affected (Avci & Karagoz, 2003:948–950). Thus, by increasing this dimension, an increase in the collection efficiency is obtained up to a certain point, where after the efficiency will decrease, depending on the flow conditions. Thus, the longer the cyclone is, the longer the residence time will be, allowing the particles to be removed in time.

Kaya and Karagoz (2009:43) experimented with extending the dipleg (Figure 12) of a CS. Similar to an optimum cyclone height, there is also an optimum dipleg length that will ensure optimum particle separation. Their calculations indicated that the dipleg performed at its best when the length was approximately 50% of the cyclone's height. If the dipleg is too long, the vortex will not reach the bottom of the dipleg or hopper effectively, resulting in poor efficiencies. Note that not all of the cyclones have a dipleg as most of them are directly connected to a dust collector or hopper.

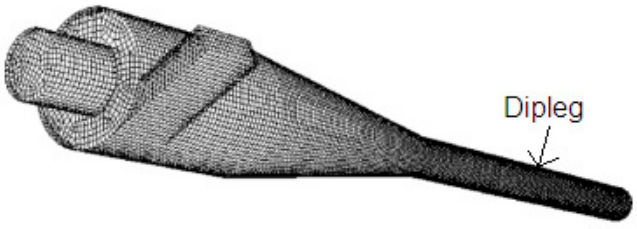

Figure 12: Dipleg of a cyclone separator

Xiang *et al*. (2001:560) conclude that the dust outlet size (B_c in Figure 5) affects the collection efficiency. From experimental results, it was found that if the dimension B_c is reduced, the collection efficiency will increase. If B_c is smaller than the gas outlet tube (D_e in Figure 5), the result will be increased collection efficiency but a greater pressure loss. If pressure drop is a concern within a CS, Xiang *et al*. demonstrate that increasing B_c will result in a lower pressure drop.

2.4.5 Multi-inlet designs

In addition to the geometry of a CS, the inlet design directly affects collection efficiency. Zhao *et al*. (2004:48) used three identical CSs with differing inlets in their study. Figure 13 depicts these different inlets:

- Figure 13 (a): Model A of the conventional single tangential inlet;
- Figure 13 (b): Model B with two conventional inlets symmetrical to each other; and
- Figure 13 (c): Model C with an inlet similar to that of Model B but which converges.

From their findings, it was noted that Model C had the best overall collection efficiency followed by Model B and then Model A. Collection efficiencies between the different models were more prominent at lower inlet velocities than at higher inlet velocities. Model C had greater collection efficiency with smaller particle sizes, making it a viable option for submicron particle removal. The downside of these more complicated inlets is a higher design and manufacturing cost and a slight increase in pressure drop (Zhao *et al*., 2004:50).

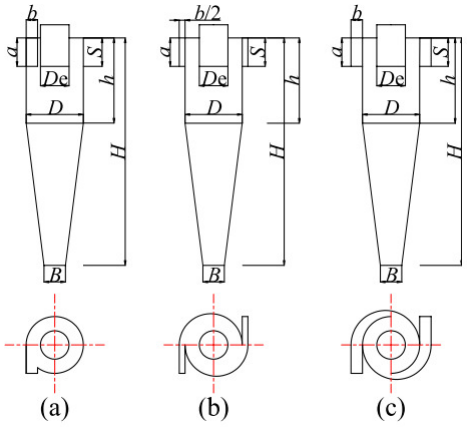

Figure 13: Alternative design inlets: (a) conventional single inlet; (b) direct symmetrical inlet; and (c) converging symmetrical inlet (Zhao *et al.*, 2004)

2.4.6 Angled inlet design

The collection efficiency of the inlet designs shown in Section 2.4.5 is also dependant on the entry angle into the CS. Qian and Wub (2009:1) tested a cyclone with different angled inlets with angles of 0°, 30° and 45°. Figure 14 demonstrate the way this inlet angle was measured. Two different velocities are taken into account when evaluating the performance of a CS: tangential and axial velocities. The tangential velocity contributes to the centrifugal force that is applied on the particle and the greater that force is, the quicker the particle will move to the cyclone wall, where it can be transported to the hopper for removal. If the axial velocity increases, the particles move more rapidly towards the hopper.

According to Qian and Wub (2009:4), the axial velocity increases as the inlet angle increases, but the tangential velocity decreases marginally on the inner vortex while it increases on the outer vortex of the cyclone. Thus, the angled inlet increases the velocity near the wall of the cyclone and for this reason the modified angle inlet results in greater collection efficiency. There is an optimum angle for the best efficiency. Fortunately, the pressure drop decreases when the angle is increased. According to Qian and Wub, this is due to reduction of swirling flow at the inlet of a CS.

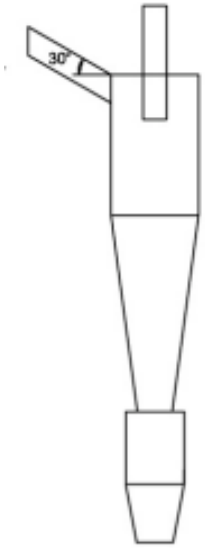

Figure 14: An angled inlet of 30°

2.5 Alternative solutions used to optimise collection efficiency

There are alternative methods that can enhance the cyclones collection efficiency without changing the CS. These methods are mainly add-ons that do not change the cyclone's geometry or set-up very much. The focus of these methods is mainly on increasing agglomeration of the particles or more efficient use of the energy available in order to enhance the CS collection efficiency.

2.5.1 Post cyclone

According to Jo *et al*. (2000:97), the idea behind a post cyclone (PoC) is to increase the collection efficiency for the particles below 5 to 10 µm. This is the main weakness of a CS as the collection efficiency of particles below 10 µm is low. A PoC has several advantages that make it very attractive, namely simple design, low capital cost, easy maintenance, low pressure drop and recovery of product dust. The last advantage applies to processes for which product dust needs to be retrieved before it is contaminated in the final filter, for example the pharmaceutical industry. Recovery of product dust also reduces the amount of particles that can block the final filter, which is beneficial to many particle removal systems, for instance the CVD soot removal system.

The PoC can be installed without tampering with the main cyclone. Ray *et al*. (1998:40) used the swirl present at the gas outlet of a CS to remove even more particles that escaped the cyclone. The PoC

consists of two cylindrical pipes fitted over each other with an annular gap between them. The PoC is fitted onto the gas outlet (vortex finder) of the CS as seen in Figure 15 on the right-hand side.

The particles that escape the CS through the gas outlet (vortex finder) will still have kinetic energy that can be used to filter the particles with the aid of a PoC. The theory behind a PoC is demonstrated on the left-hand side of Figure 15. These particles collide against the inner shell in a spiral motion and when they reach the annular gap at the top, some of the particles enter between the inner and outer shells in which they are trapped. The right-hand side of Figure 15 shows a PoC outlet that is used to bleed the PoC. This outlet can be reconnected to the final filter or the CS.

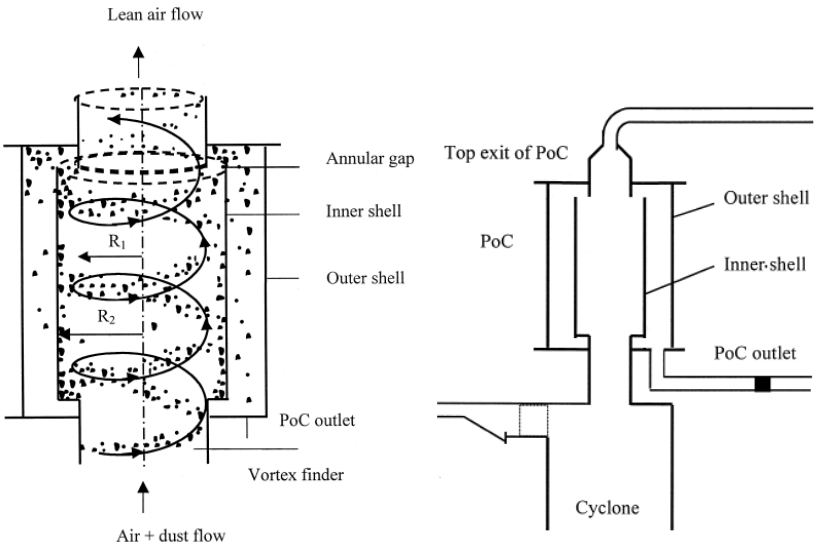

Figure 15: Post cyclone operation (left) and fitting (right) (Joe et al. 2000)

The PoC showed an increase in efficiency with an increase in bleeding, as measured by Ray *et al*. (1998:43) and calculated by Jo *et al*. (2000:102,105). The overall efficiency was improved by 2 to 20%, depending on the operating conditions and the CS size. The smaller the CS is, the less impact the PoC has, owing to the higher efficiency of smaller particles in smaller cyclones. According to Jo *et al*. (2000:107), the PoC causes a pressure drop of about 10%, independent of the bleed percentage. Through the use of CFD simulation, Ray *et al*. (1998:42) demonstrate the way the recirculation effect occurs in a PoC and suggest that this can increase agglomeration and impaction of the particles.

2.5.2 Adding external flow

The addition of an external flow works on the principle that an additional stream is introduced tangentially to increase the rotational velocity of the gas inside the CS. This method decreases the 50% cut size (see Section 2.3.3) for submicron particles; that is, it enhances collection efficiency. Subsequently, the additional inlet into the cyclone results in the removal of smaller-sized particles due to the higher centrifugal force applied (Yoshida *et al.*, 2009:6). Figure 16 demonstrates the additional input through inlet *q*, which operates in a manner similar to the direct symmetrical inlet as mentioned in Section 2.4.5. The only difference is that clean gas is introduced into one inlet *q* from a secondary independent source, such as a compressor or blower.

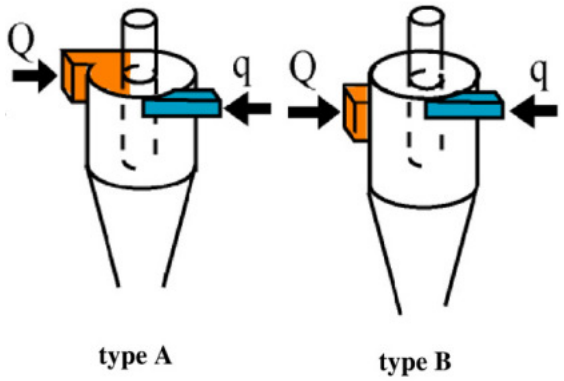

Figure 16: Increased velocity by external flow

Experiments on the additional inlet *q* at different heights above the cyclone inlet *Q* found that Type B in Figure 16 has a higher efficiency than Type A (Yoshida *et al.*, 2009:7). The higher positioned additional inlet *q* in type B increases the downward velocity more than that of type A and causes the particles to move nearer to the wall region of the cyclone. Another reason for this higher efficiency is that the vortex starts to form above the inlet *Q*, if additional inlet *q* is above inlet *Q* where the particles enter. This reduces eddy currents and causes the particles to move more rapidly to the dust outlet (Yoshida *et al.*, 2009:11).

2.6 Soot

It is beneficial to examine and understand the substance that needs to be removed by a CS. Knowing the characteristics of soot and how it agglomerates can result in an improved CS design and model. Therefore, these sections examine the structure and formation of soot, as well as agglomeration.

2.6.1 Formation and structure

Soot formation occurs when a hydrocarbon-based fuel is combusted in a low-oxygen environment. It can be described as the incomplete combustion of a hydrocarbon fuel (such as alkane, alkene, alkyne, cycloalkane and alkadiene). When hydrocarbon fuel combusts in a low-oxygen environment, it leads to the formation of benzene-like rings and chains that form PAHs with higher molecular weight. This can be seen in Figure 17 from the bottom at time zero to the top about 50 ms later. These PAHs undergo polymerisation until the primary particle is formed that is normally in spherical form. These particles then cluster together through surface bonds and aggregate into larger particles that eventually agglomerate into the macroscopic soot structures. These soot particles can undergo oxidation and agglomerate further into sizes ranging from 50 nm to 10 µm.

Soot is found in various forms, such as amorphous carbon, fullerene carbon or quasi-crystalline carbon, while the elemental soot particle can correlate with black carbon (BC). Even though the soot surface nanostructures and elemental composition may differ from one another, many correlations and similarities can be drawn in terms of the primary particle sizes and the formation of particle agglomerates (Murr & Soto, 2005:50).

These different structures mentioned above can be in the form of overlapping flat segments of PAHs or hexagonal graphitic sheets or closed-shell formations formed by curved graphene layers. According to Murr and Soto (2005:50), these closed-shell formations can be categorised into onion-like structures, concentric fullerene polyhedra or tube formations, which can be single-wall capped with half a fullerene molecule and multi-wall capped with concentric fullerene known as *polyhedral hemi-shells*. Vander Wal and Tomasek (2004:131) demonstrate that fuel composition, combustion temperature and kinetics, and chemistry play a role in the soot structure. They formed soot during thermal pyrolysis of different fuels, namely acetylene (C_2H_2) and ethylene (C_2H_4) mixed with helium, at low temperatures and found that it produced amorphous structures. At higher temperatures, the soot yielded different nanostructures compared to lower temperatures, while flow

rates were varied. It was found that high flow rates produced carbon shells and capsules within the soot spherules (graphene) and at lower flow rates the segments were oriented parallel to each other with a more graphitic soot character.

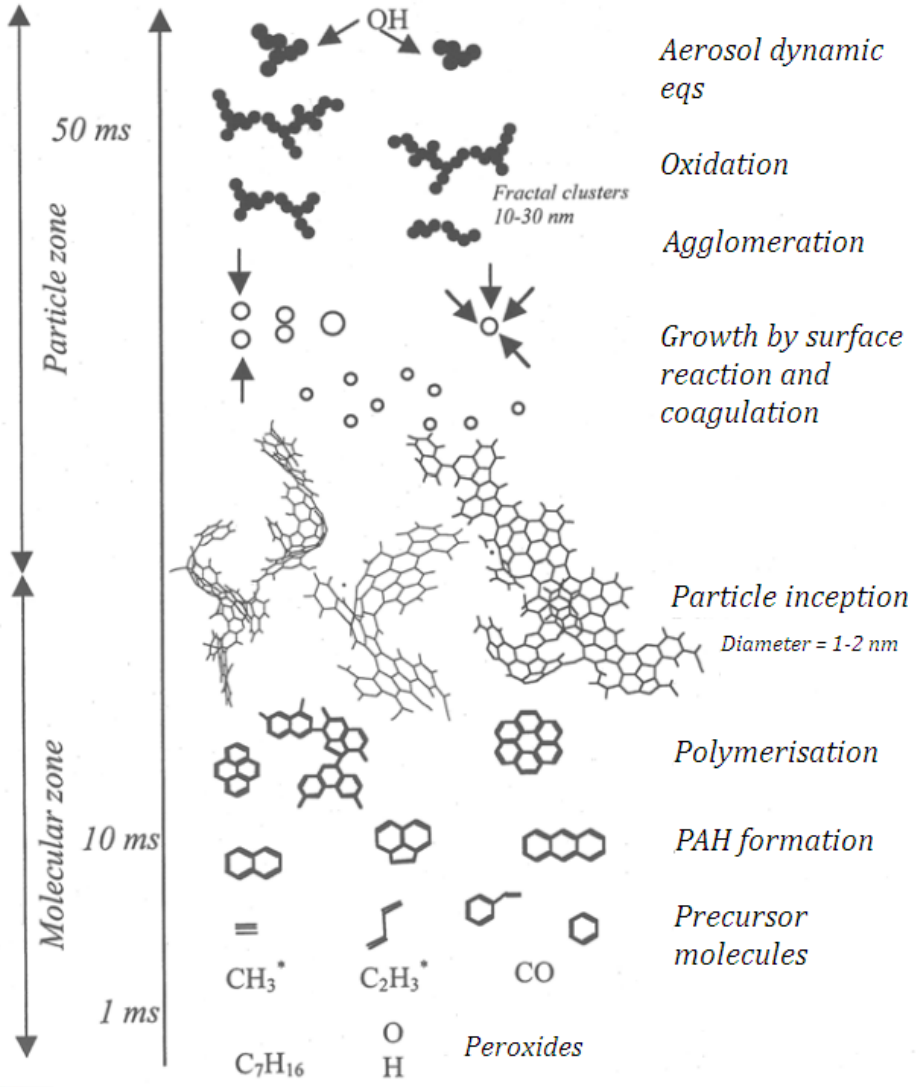

Figure 17: Soot formation (Pugmire et al., 2003)

2.6.2 Agglomeration and aggregation

Debate on the terms *agglomeration* versus *aggregation* led to controversy in recent decades. These terms, according to Nichols *et al*. (2002), were interchanged over the past few years. Table 3 below presents the recent changes to the meanings of these terms as summed up by Nichols *et al*. (2000). The ISO standard will be used for the purpose of this mini-dissertation, but it should be noted that Nichols *et al*. (2002) suggest that the terms hard and soft agglomerate be used to describe the bondage between the particles.

Table 3: Use of the terms *agglomerate* and *aggregate* from seven literature sources

Source (quoted by Nichols *et al*., 2000)	Assemblage of particles that is loosely bound with particles that are loosely attached by contact at their corners and edges. Readily dispersed	Assemblage of particles that is rigidly bound with particles that are firmly attached at their faces by fusion, sintering or growth. Not readily dispersed
BS 2955: 1993	Aggregate	Agglomerate
ISO 14887	Agglomerate	Aggregate
USP 24 2000 (Monograph 776)	Aggregate	Agglomerate
Chambers Science and Technology Dictionary (1988)	Aggregate	Agglomerate
A. Van Hook (1961)	Aggregate	Agglomerate
W. Gerstner (1966)	Agglomerate	Aggregate
J.W. Mullin (1993)	Agglomerate	

As mentioned in Section 2.6.1, similarities can be drawn between different soot particles in terms of agglomeration and particle size. Figure 18 and Figure 19 (Murr & Soto, 2005:51) depict a transmission electron microscopy (TEM) image of BC and diesel soot aggregate. It is evident that there are similarities in agglomeration and particle size. The main advantage of these similarities is that agglomeration theories that apply for diesel soot can be generally applied to much of the different soot available.

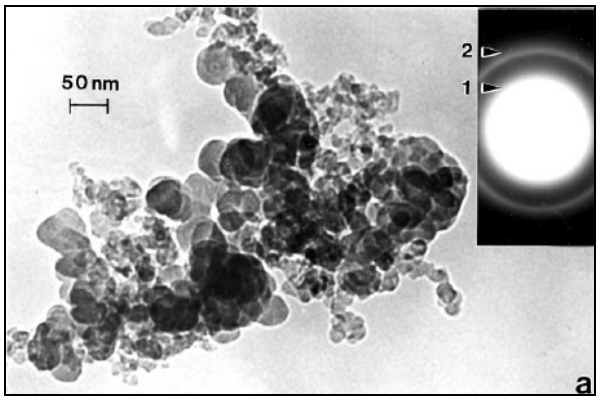

Figure 18: Black carbon aggregate

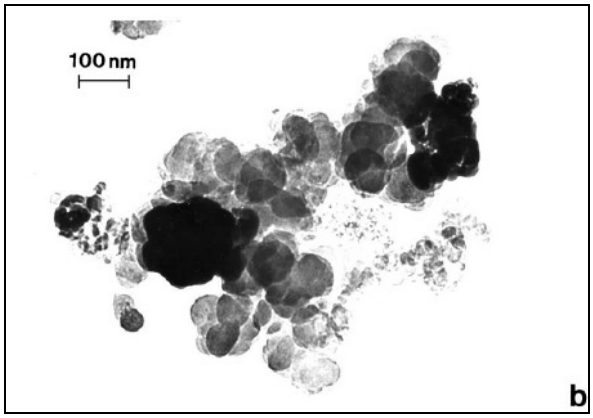

Figure 19: Diesel soot aggregate

There are five types of forces that can agglomerate (Fayed & Otten, 1984:231) particulate matter (PM), namely solid bridges, interfacial forces and capillary pressures at freely movable liquid surfaces, adhesion and cohesion forces with unmovable binder bridges, attraction forces between solid particles, and form-closed bonds (interlocking).

1. Solid bridges are classified by chemical reaction, crystallising of dissolved substances or solidification of melted substances. These solid bridges mostly occur at high temperatures as occur during the CVD process.
2. Interfacial forces and capillary pressures at freely movable liquid surfaces can create strong bonds if the liquid does not evaporate. These are mainly the forces inside a scrubber using water to agglomerate the PM.
3. Adhesion and cohesion forces with unmovable binder bridges result from the use of a binder that has a very high viscosity. This forms bonding similar to solid bridges and occurs when using a substance such as tar. The highly viscous substance forms a layer around the PM that allows smaller particles to be trapped.
4. Attraction forces between solid particles generally include van der Waals-, electrostatic- or magnetic forces. These forces only apply when the particles are close to each other, and the smaller particles benefit mostly from these forces. Soot generally falls in this category.
5. Form-closed bonds apply when the matter can interlock with itself and other matter physically, such as fibres locking or folding around each other.

Soot, which generally consists of small particles, will generally agglomerate owing to orthokinetic interaction. When these small soot particles collide, van der Waals forces attract these particles to one anther, thus causing agglomeration. There are many different approximations for calculating the van der Waals forces but the most popular approach is that given in equation (2.6.2.1) below (Fayed & Otten, 1984:236). In the equation, the adhesion force (inter-particle bond strength) F_v is proportional to the primary particle diameter d (assuming spherical particles) and inversely proportional to the squared distance. The constant c differs in the various models, for example Liefshifz–van der Waals Constant is $\frac{\hbar\varpi}{16\cdot\pi}$.

$$F_v = c.\frac{d}{a^2} \qquad (2.6.2.1)$$

In order to obtain an estimated tensile strength of an agglomerate, it is to be assumed that the particles are equally sized and of spherical form, based on the statistical considerations of Rumpf

(Bika *et al.*, 2001:107; Fayed & Otten, 1984:233). The tensile strength of an agglomerate can determine the extent to which it can easily fragment. Thus, the stronger the tensile strength of an agglomerate is, the better the agglomerate will hold and not de-agglomerate.

Equation (2.6.2.2) yields tensile strength σ_t, where ε is the porosity of the agglomerate or the specific void volume, and Q is the average coordination number of the packed spheres:

$$\sigma_t = \frac{(1-\varepsilon)}{\pi} \cdot \frac{QF}{d^2} \qquad (2.6.2.2)$$

Substituting equation (2.6.2.1) into equation (2.6.2.2) yields the tensile strength for the van der Waals forces.

$$\sigma_{tv} = \frac{(1-\varepsilon)}{\pi} \cdot \frac{Qc}{a^2} \cdot \frac{1}{d} \qquad (2.6.2.3)$$

From equation (2.6.2.3), it can be seen that the agglomeration forces depend on the particle size and distance between the particles. Thus, the smaller the particle diameter *d* is and the smaller distance between the particles a is, the greater tensile strength due to van der Waals forces will be. The same calculation can be made for all the inter-particle forces mentioned as the five types above. For this, only *F* would be substituted with the applicable force's formula.

Figure 20 shows a scanning electron microscope (SEM) image of soot that was collected in the ACF at Pelindaba, South Africa. The soot shows remarkable agglomeration. The bond strength of the soot is unknown and thus it is difficult to predict the extent to which the agglomerate will hold together in high flow rates. The SEM images confirm that the effect of agglomeration on CS collection efficiencies should be considered.

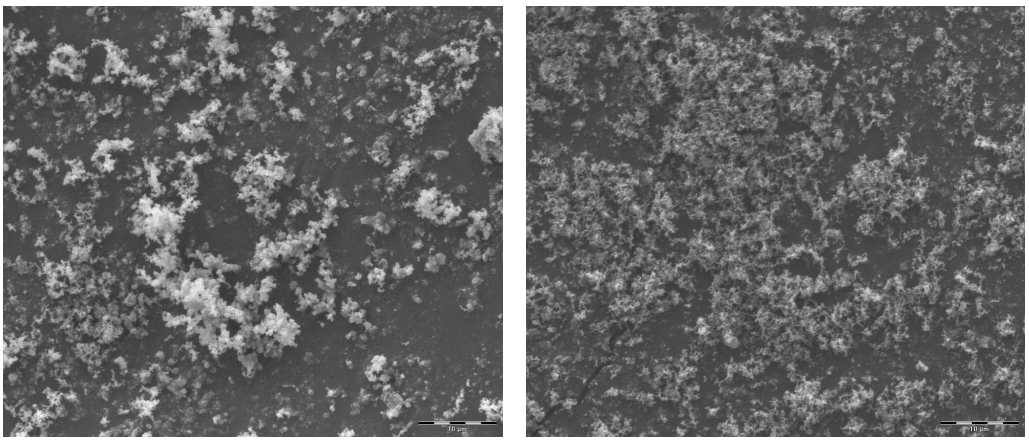

Figure 20: Advance Coater Facility soot scanning electron microscope image (University of Potchefstroom, 2009)

2.7 Techniques for agglomerating soot

The following sections discuss methods of amplifying agglomeration of particles. This will increase the average particle sizes and therefore increase the total collection efficiency of CS.

2.7.1 Acoustic agglomeration

Acoustic agglomeration is an attempt to increase the general particle size before the separation or filtration stages. An increase in particle agglomeration leads to a higher collection efficiency for both filters and cyclones. In an experiment by Lui *et al*. (2009:6), fly ash from a coal-fired plant was collected from an electrostatic precipitator and fed into an acoustic chamber with a horn on the one side. This horn was connected to a signal generator with a range of 180 to 5500 Hz that used an 80 W amplifier to generate sound of up to 150 dB. Their experiment yielded a reduction of 68% in independent particle clusters when using a sound pressure level (SPL) of 147 dB and a frequency of 1400 Hz (Lui *et al*., 2009:12). This result was observed using a PSD meter and SEM images of the pre- and post-acoustic agglomerated fly ash. Figure 21 (Lui *et al*., 2009:22) presents the SEM images of the agglomerated of fly ash before (on the left-hand side) and after (on the right-hand side).

Lui *et al*. (2009) identified four influential parameters, namely frequency, residence time, SPL and higher initial number concentration. Firstly, there is an optimal frequency for different PSDs and from the experimental results it was discovered that a higher SPL led to a lower optimum frequency.

Secondly, the longer these particles are exposed to the acoustic agglomeration process, the larger the agglomerate. Thirdly, a higher SPL value complements the agglomeration process with a minimum value of 140 dB; below this value no significant effect was observed. Lastly, a higher initial number concentration implies that the particles are closer together and will therefore agglomerate better. The acoustic agglomeration method can be used instead of the electrostatic precipitator process that may ignite explosive gases such as hydrogen.

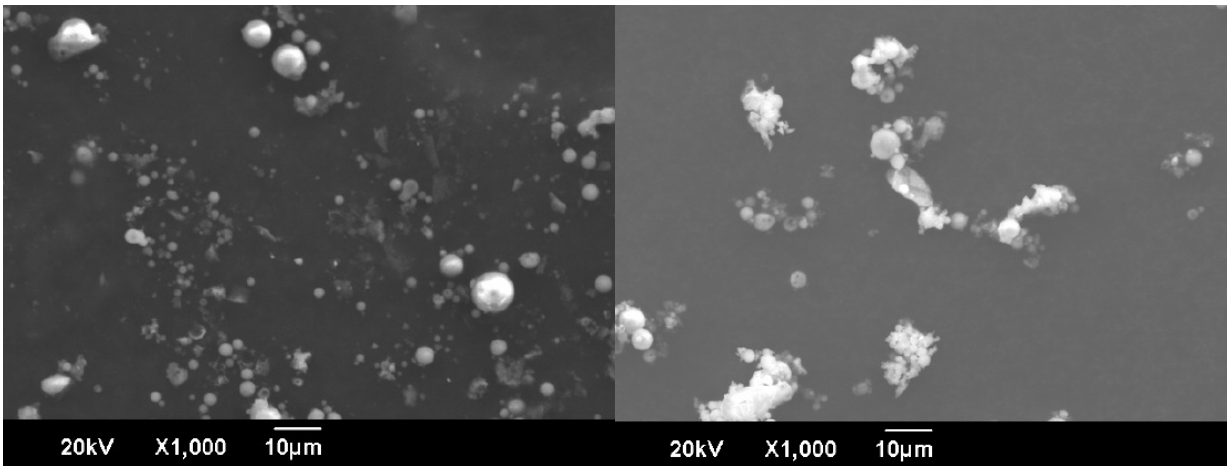

Figure 21: Acoustic agglomeration before (left) and after (right), (Lui *et al*., 2009:22)

2.7.2 Coulomb interactions

Onischuk *et al*. (2000:S948) found that approximately 50% of all the soot generated (from burning propane) had an electrical charge. This means that an electric field can be used to manipulate the soot to increase the agglomeration rate. They observed that some particles have either a positive or a negative charge and some have no charge at all. Figure 22 demonstrates the agglomeration of soot in an electrical field. This TEM image, if read from left to right, demonstrates the agglomeration of a particle over time intervals of 0.04 s. Onischuk *et al*. (2000:S949) conclude from their experiment that electrical charge will influence the dynamics of the soot agglomeration process.

Figure 22: Agglomeration via electric field (Onischuk *et al*., 2000:S949)

2.7.3 Moistening soot

A third alternative to increased agglomeration is to inject mist into the cyclone. The mist will increase the interfacial tension (Section 2.6.2) between the particles, thereby increasing the particle size and making the cyclone more efficient. Yang and Yosida (2004:222–223) conducted an experiment with two similar sized cyclones in which only the position of the mist inlet differed. Figure 23 shows that the mist inlet of Type B was placed 4 mm from the wall instead of against the wall as with Type A. They argue that Type B will have lower wall mist loss than that of Type A. When lower mist loss occurs, more particles are affected by the mist and therefore the likelihood of the particles agglomerating increases.

Yang and Yosida (2004:230) conclude that the Type B design was more effective than the Type A, even if air without mist was injected, which correlates to the multi-inlet design as discussed in Section 2.4.5. Their overall conclusion is that the mist reduced the 50% cut size (Section 2.3.3) of the particles for both Type A and B designs. The position of the different inlets affected collection efficiency as well. Moist injection causes the particles captured to from a sludge solution inside the cyclone's collector bin, which makes it difficult to clean.

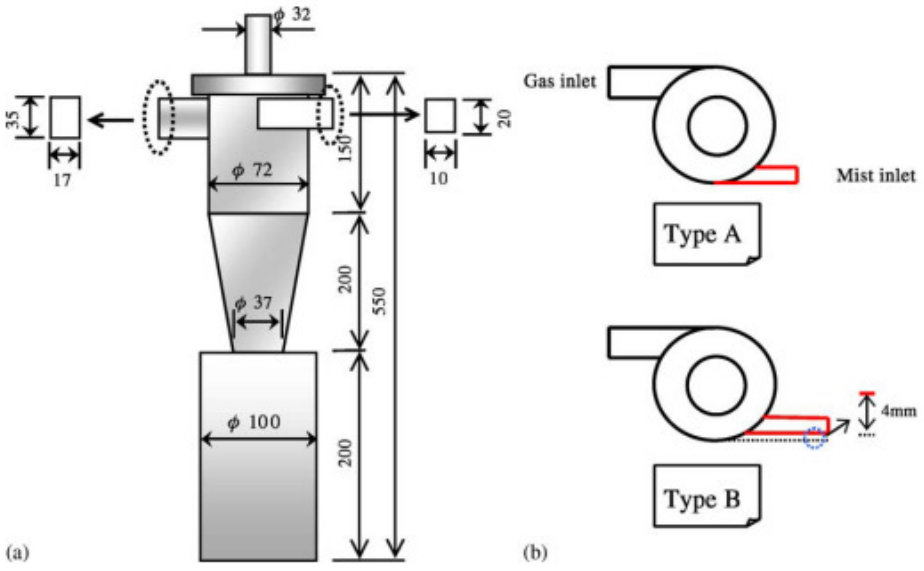

Figure 23: Mist injection with inlets varying 4 mm

2.8 Chapter summary

This chapter has reviewed the literature that has informed this project. Background information, regarding the project has been given and information about CS design and operation has been examined. The effect that different operating and design parameters have on CS has been discussed, for example increasing the flow rate or decreasing the inlet size. Alternative solutions have been investigated, ranging from external add-ons as PoCs, external additional flow, mist injection and electrostatic precipitation. A variety of experiments conducted on CSs has been reviewed, in order to comprehend their operation. Soot has been studied regarding the formation and agglomeration of soot particles. Techniques that could increase the agglomeration of soot have been investigated as well, for example the acoustic agglomeration process. The next chapter will discuss the theoretical model used to predict the collection efficiencies of the CSs.

CHAPTER 3: MODELLING METHODOLOGY

3.1 Introduction

This chapter focuses on the model used to predict the collection efficiencies of the newly designed cyclones. The challenges of selecting a suitable model are two-fold: firstly, data availability; and secondly, the availability of resources (time, financial support) to complete a design. Data availability mostly relies on the equipment available to obtain certain parameters, for example flow patterns, pressure drops at different parts inside the CS or an accurate in-time particle size distribution (PSD) of the particles entering and exiting the cyclone. Designing a cyclone with the aid of CFD modelling was unfortunately not possible for this project, owing to the time and cost constraints regarding CFD programming. This chapter explains the implementation and calibration of the model with the given data.

3.2 Data availability

The data for this project was obtained from the ACF design and included:

- dimensions of both the previous and newly designed cyclones;
- typical flow rates of the gases with their characteristics (viscosity, density); and
- a PSD logarithmic graph of the soot produced.

The data is explained in the following sections.

3.2.1 Advance Coater Facility cyclone dimensions

The cyclone dimensions were obtained from drawings. An isometric view of this is shown on the left-hand side of Figure 24. The ACF tested different mechanisms to remove soot trapped inside the CS. The piston arm on the top of the ACF cyclone was used to scrape off dust from the walls inside the CS. Unfortunately, the plates shown on the right-hand side of Figure 24 disturbed the vortex inside the CS and reduced its collection efficiency. The ACF cyclone uses a circular inlet. The circular inlet was approximated with a square of the same area because the model required a value for

dimensions *a* and *b* in Figure 5 and Figure 24. This approximation was only conducted in order to obtain values for *a* and *b*. There was no need to use the hydraulic diameter as the model is not dependant on Reynolds number owing to the assumptions made for the friction coefficient f and the turbulent diffusion coefficient D_r, in Section 3.3.1. The inlet pipe was 60.33 mm in diameter. The steel thickness was 4 mm, which reduced the pipe's diameter to 52.33 mm. Applying a simple calculation yielded the length of a square as 46.38 mm, which was used to approximate the circle's area. The remaining dimensional values were simply obtained from the drawings by subtracting the steel thicknesses.

Table 4: Advance Coater Facility cyclone dimensions (in metres)

a	b	B_c	D_c	D_e	h	H_c	S
0.04638	0.04638	0.308	0.492	0.07366	0.302	1.081	0.188

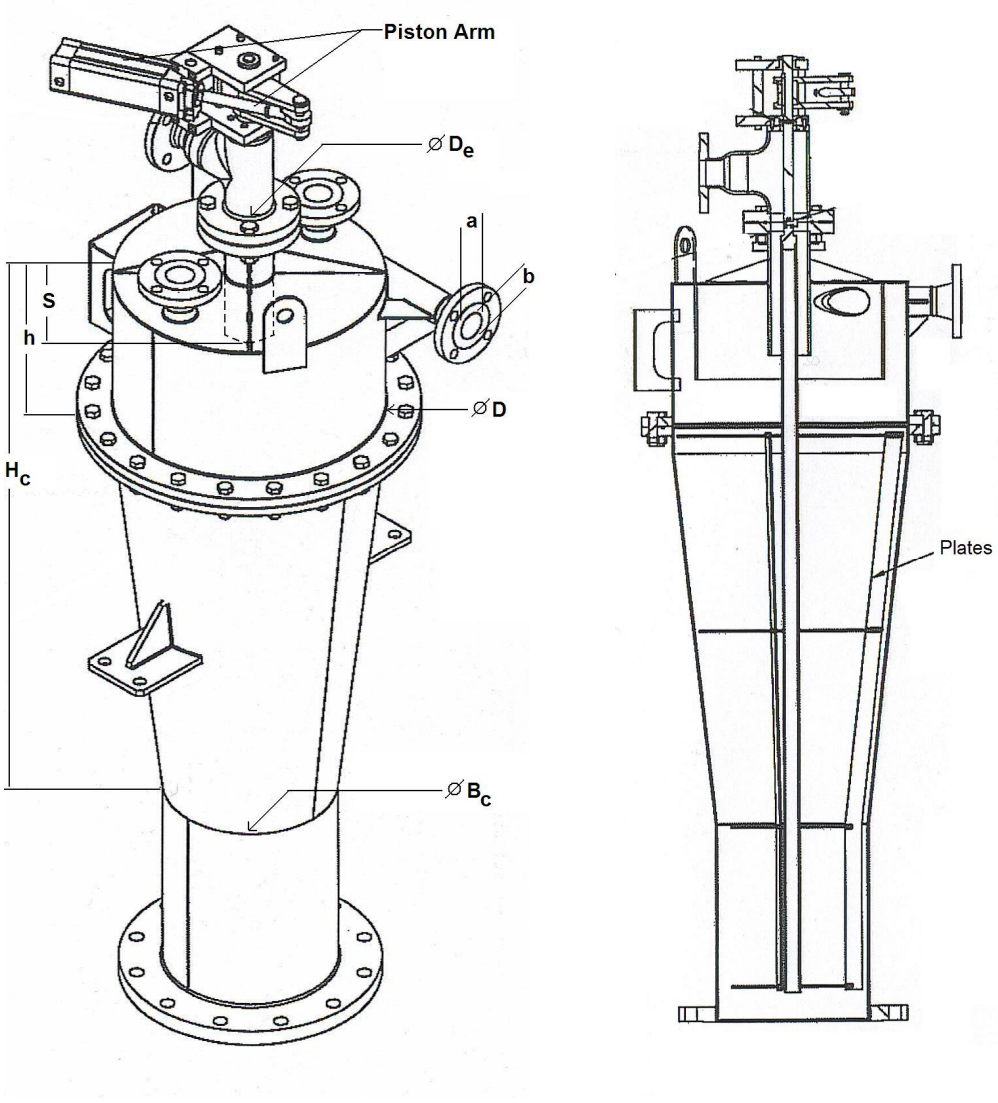

Figure 24: Advance Coater Facility cyclone dimensions including the piston arm (left) and the internal cross-section depicting the scrape plates (right)

3.2.2 Operating conditions

The operating conditions provided were assumed to remain the same for the newly designed cyclones. All the values that were used during the operation of the ACF cyclone, given in Figure 24, are tabulated in Table 5 on the next page. The values of the major contributing parameters are given in bold. Each of those parameters has a direct impact on the efficiency of the cyclone and they were

thus used in the model. The remainder values, for example the Argon and Hydrogen flow rates, were used to calculate total process off-gas flow rate. The same was done to calculate the viscosity and density of the mixed process gases. It was assumed that these values were measured at the inlet of the cyclone. The total collection efficiency was calculated by measuring the captured soot from the first and second cyclones and the final bag filter as was illustrated in Figure 3. A simple mass balance equation determined the efficiency of the cyclone, as it was assumed that the final bag filter captured the remaining soot balance. Therefore, the sum of the two cyclones with the bag filter yields the total amount of soot.

Table 5: Operating conditions

Property	Unit	Values
Temperature	°C	**60**
Pressure	kPa	87.94
Mass flow rate		
Argon mass flow rate	kg/h	61.42
Hydrogen mass flow rate	kg/h	2.026
Process off-gas mass flow rate	kg/h	63.446
Volume flow rate		
Argon volume flow rate	m^3/h	48.41
Hydrogen volume flow rate	m^3/h	31.67
Process off-gas volume flow rate	m^3/h	**80.06**
Density		
Argon density	kg/m^3	1.269
Hydrogen density	kg/m^3	0.06397
Process off-gas density	kg/m^3	**0.7925**
Viscosity (x 10^{-6})		
Argon viscosity	kg/m-s	24.921
Hydrogen viscosity	kg/m-s	9.782
Process off-gas viscosity	kg/m-s	**24.096**
Soot data		
Mass flow rate	kg/h	9.737
Concentration	g/m^3	**121.6**
Cyclone total collection efficiency	%	**60.2%**

3.2.3 Particle size distribution

The PSD is very important for obtaining an accurate grade efficiency curve. The PSD is presented in Figure 25. Graph B on the right-hand side of the figure indicates the particle size range (that is submicron < particles size (*d*) < approximately 20 µm) and Graph B is obtained by integrating Graph A. Therefore, Graph A on the left-hand side of the figure represents the particle sizes with their relative abundance or fraction and the integral of this graph should deliver 100% or 1. In order to simplify calculations, this graph was discretised, the result of which is given in Figure 30. Elemental particle density was assumed to be 1800 kg/m³, an average value for soot from Hong *et al*. (2005:14). Figure 25 depicts the actual PSD of the ACF cyclone measured by the company called THERMTRON. Approximately 24% of the particles will be between 8 and 10 µm in size. The PSD in *Graph A* was codified as seen in Figure 30 and the exact values are depicted in the first two columns of Figure 36.

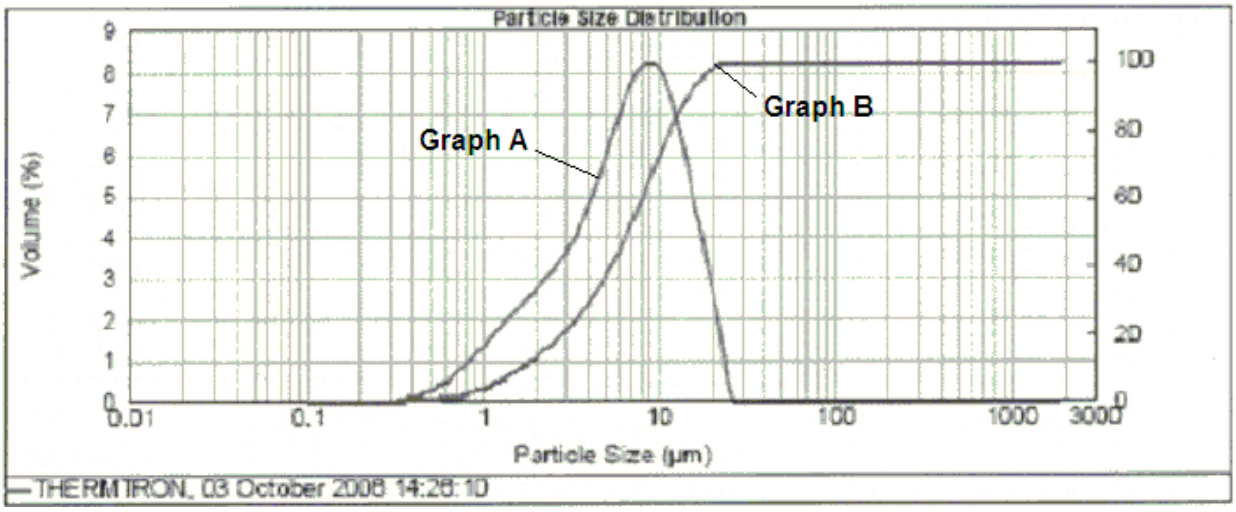

Figure 25: Particle size distribution of the soot at the inlet of the cyclone

3.3 Theoretical model

According to Gimbun *et al*. (2004:42–43), the most accurate model by which to predict collection efficiency is Li and Wang's model. This model's required input parameters are adequate when compared with the data available from the ACF cyclone. Therefore, Li and Wang's model was used in this project to predict the collection efficiencies of the newly designed cyclones. The model is explained in the following sections.

3.3.1 Li and Wang model

A model that still uses the basic inputs as previously mentioned is Li and Wang's model (1989:668). This model includes particle bounce or re-entrainment of particles and turbulent diffusion near the CS wall. Previous models, such as Leith and Licht's model assume that the particle concentration within the cyclone is uniformly mixed; however, Wan *et al*. (2008:97) found that different sized particles have different positions, as was depicted in Figure 6. Li and Wang's model does not assume uniform radial concentration or a constant radial particle velocity for the uncollected particles inside the CS, which enhances the prediction confidence of the model.

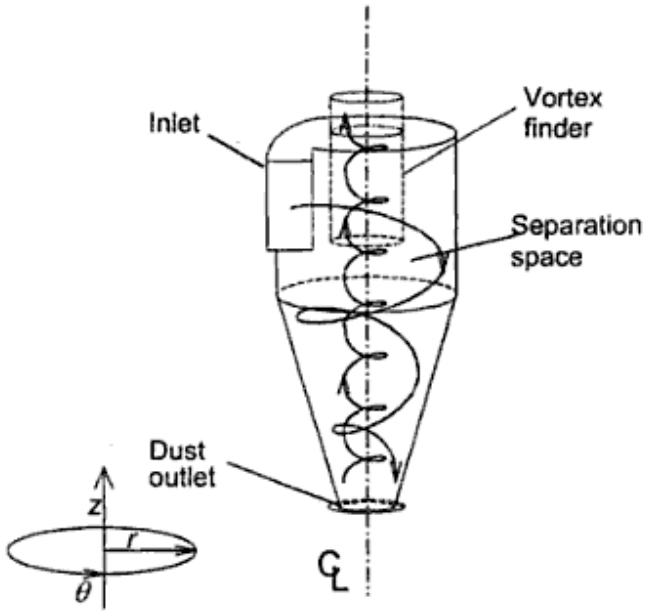

Figure 26: Cyclone coordinates: tangential (θ), radial (*r*) and axial (*z*)

Figure 26 illustrates the coordinate system for a CS, in which the tangential (*θ*), radial (*r*) and axial (*z*) components are depicted in the lower-left corner. An example of coordinate gas velocities is shown in Figure 27, in which (a) is the tangential velocity, (b) is the radial velocity and (c) is the axial velocity.

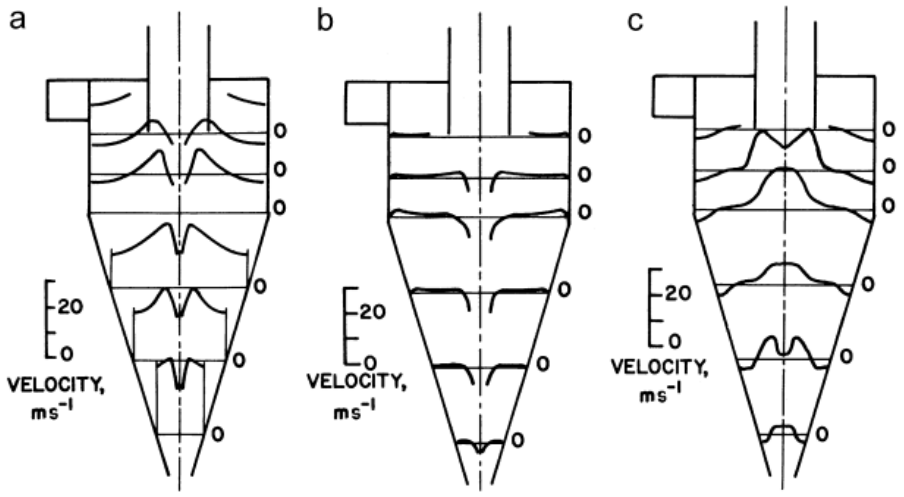

Figure 27: Example of velocity components in a cyclone separator: (a) tangential; (b) radial; and (c) axial

Firstly, Li and Wang disregarded the turbulent diffusion inside the CS and the particle settling velocity in the *z* direction. The equations of continuity and the conservation of particles led to a new model for particle distribution inside the CS, given as:

$$w\frac{\partial c}{\partial r}+u\frac{1}{r}\frac{\partial c}{\partial \theta}=0\text{, for } 0\le\theta\le\theta_1 \qquad (3.3.1)$$

Secondly, they took the boundary conditions into account with the turbulent diffusion coefficient D_r and the particle bounce re-entrainment on the cyclone walls, α will yield:

$$D_r\frac{\partial c}{\partial r}=(1-\alpha)wc\text{, at } r=D_c/2 \qquad (3.3.2)$$

where the expression for D_r is:

$$D_r=0.052R_c u\sqrt{f/8} \qquad (3.3.3)$$

Li and Wang (1989:667) assume 0.02 for the friction coefficient f, where u is the inlet velocity in equation (3.3.3). The radius R_c can be calculated as follows:

$$R_c = (D_c - D_e)/2 \qquad (3.3.4)$$

The concentration of particles *c* at the angular coordinate $\theta = 0$ is equal to the inlet concentration c_0.

$$c = c_0, \text{ at } \theta = 0 \qquad (3.3.5)$$

Li and Wang derived an expression, given in equation (3.3.6), for the radial particle velocity w, by calculating the centrifugal force due to the gas stream and the effect of the drag force due to the radial gas velocity (assumed Stokes' drag). Assuming the tangential velocity ur^n is constant, the equation is given by:

$$w(r) = (\rho_p - \rho_g)u^2 d^2 \big/ 18\mu r \qquad (3.3.6)$$

where ρ_p and ρ_g represent particle and gas density, respectively; u is the tangential component of the gas velocity in the cyclone vortex; and *d* is the particle diameter. For the vortex exponent n, an empirical expression proposed by Alexander was used (this is valid for any cyclone diameter and gas temperature):

$$n = 1 - [(1 - 0.67 D_c^{\,0.14})(T/283)^{0.3}] \qquad (3.3.7)$$

Li and Wang (1989:667) used the vortex exponent to calculate the tangential component of the gas velocity in the cyclone vortex as:

$$u(r) = \frac{(1-n)Q}{b(r_w^{1-n} - r_n^{1-n})r^n} \qquad (3.3.8)$$

In order to obtain the final concentration distribution inside a CS, the equations above are solved to yield:

$$c(r,\theta) = \frac{c_0(r_w - r_n)\exp\left\{-\lambda\left[\theta - \dfrac{1}{K(1+n)}r^{1+n}\right]\right\}}{\displaystyle\int_{r_n}^{r_w}\exp\left[\frac{1}{K(1+n)}r^{1+n}\right]dr} \qquad (3.3.9)$$

where

$$r_w = D_c / 2 \text{ and } r_n = D_e / 2$$

Using the definition of fractional efficiency (see equation 2.3.3.2), the collection efficiency can be calculated by measuring the concentration of particles that enters the cyclone (c_0) and the concentration leaving the cyclone (c_1). The difference between these values will determine the total collection efficiency as:

$$\eta = 1 - \frac{c_1(\theta_1)}{c_0} \qquad (3.3.10)$$

The average particle concentration at c_1 is calculated using equation (3.3.9) and is given by:

$$c_1 = c_0 \exp(-\lambda\theta_1) \text{ if } \theta = \theta_1 \,\&\, r = 0 \quad (3.3.11)$$

The resultant equation from substituting equation (3.3.11) into equation (3.3.10) yields equation (3.3.12) that represents the fractional efficiency of a cyclone. This substitution makes the model independent of input and output concentrations, therefore Smolik's model as explained in Section 2.4.3 can be used if needed to compensate for variable particle concentration inputs. This compensation is only needed if the particle concentrations of soot play a major role in the total collection efficiency because of higher agglomeration. The grade efficiency is calculated from the fractional efficiency given by:

$$\eta = 1 - \exp(-\lambda\theta_1) \qquad (3.3.12)$$

where

$$\theta_1 = 2\pi(S + L) \qquad (3.3.13)$$

and *L* is the natural length, defined by Alexander as the longest distance that the vortex makes below the vortex finder (that is, where the outer vortex changes to the inner vortex). *L* was empirically measured and is given as:

$$L = 2.3D_e(D_c^{\ 2}/ab)^{1/3} \qquad (3.3.14)$$

If *L* is larger than the height of the cyclone then *L=H-S*. In equation (3.3.12), λ is defined as:

$$\lambda = \frac{(1-\alpha)Kw_w}{D_r r_w^n} \qquad (3.3.15)$$

where

$$K = \frac{(1-n)(\rho_p - \rho_g)d^2Q}{18\mu b(r_w^{1-n} - r_n^{1-n})} \qquad (3.3.16)$$

Equations (3.3.16) and (3.3.17) define λ and *K*, respectively, in equation (3.3.9). The grade efficiencies are then calculated for each particle size represented by the PSD in order to plot the resulting grade efficiency curve given by equation (3.3.12). The typical shape of these calculated curves is depicted in Figure 8 and Figure 30. The following sections discuss the limitations of and modifications made to Li and Wang's model.

3.3.2 Model limitations

Owing to simplifications made by Li and Wang (1989), there are several aspects that were not considered in order to achieve simplified calculations. As demonstrated in Section 2.4.4, several dimensions of a CS that have an effect on the collection efficiency were not taken into account by Li and Wang:

- the bottom diameter B_c or the cone tip diameter (see Section 2.4.4);
- the cyclone height H_c and cylinder height *h* (see Section 2.4.4);
- the dipleg length (see Figure 12);
- the inlet geometry, angle and location (see Sections 2.4.5, 2.4.6 and 2.5.2).

Li and Wang modified the geometry of a cyclone as shown in Figure 28, in which the natural length *L* was derived from equation (3.3.14). Experimental results from previous CS can be used to justify an outcome and thereby overcome these limitations. For example, if the cyclone has a very large

B_c / D_c value compared to other high efficiency cyclones, then based on the empirical data presented in Section 2.4.4 it can be determined that the CS will have a lower collection efficiency.

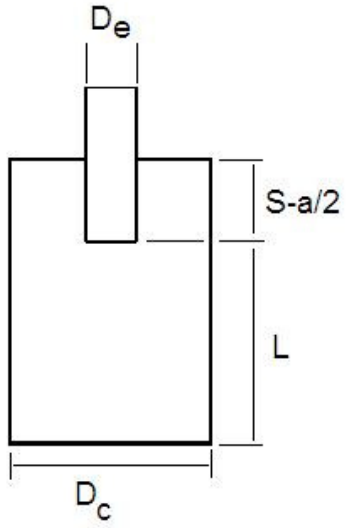

Figure 28: Li and Wang simplified cyclone geometry

3.3.3 Model modifications

Gimbun *et al*. (2004:43) found that Li and Wang's model could be improved if a modified expression for the vortex exponent *n* was used. Instead of using the original vortex exponent as given by equation (3.3.7), Gimbun *et al*. used:

$$n = 1 - [(1 - 0.5 D_c^{\,0.14})(T/283)^{0.3}] \qquad (3.3.17)$$

The result of this modification, given by equation (3.3.17), can be seen in Figure 7 and Figure 8. It was mentioned in Section 2.4.3 that Smolik's model can be used to correlate the total collection efficiency predicted by Li and Wang's's model. Ji *et al*. (2009) suggest that the lowest particle concentration that can be used with Smolik's model is 40 mg/m³ (see Section 2.4.3). Cortés and Gil (2007:428) state that the collection efficiency models will be accurate if the particle concentration is lower than 5 to 10 g/m³. Therefore, in order to account for agglomeration inside the CS due to higher particle concentration loading, equation (2.4.3.1) can be used to predict the total collection efficiency more accurately. If the soot particles are not overly dependant on concentration loading, then

Smolik's model can be disregarded. The influence of the concentration on the total collection efficiency must be experimentally verified to determine whether the soot particles follow Smolik's model. This validation cannot be conducted with the data available.

3.3.4 Model methodology

Figure 29 summarises the methodology used to obtain the final collection efficiency values. The model first uses the input data available (blocks 1 and 2), namely the physical dimensions of the cyclones and operating conditions, such as the flow rate, gas viscosities and particle densities. The input parameters were then used in the modified Li and Wang model (block 3; see Sections 3.3.1 and 3.3.3) to obtain a grade efficiency curve (block 4). The total collection efficiency (block 6) is thereafter calculated as the result of the product of the grade efficiency curve and the PSD (block 5). The efficiency calculated does not take particle concentration or agglomeration into account. Smolik's model or correlation (block 7) can be used to correct this phenomenon if required to yield a more accurate total collection efficiency (see Sections 2.4.3 and 3.3.3 for info of Smolik's model and the influence of particle concentrations).

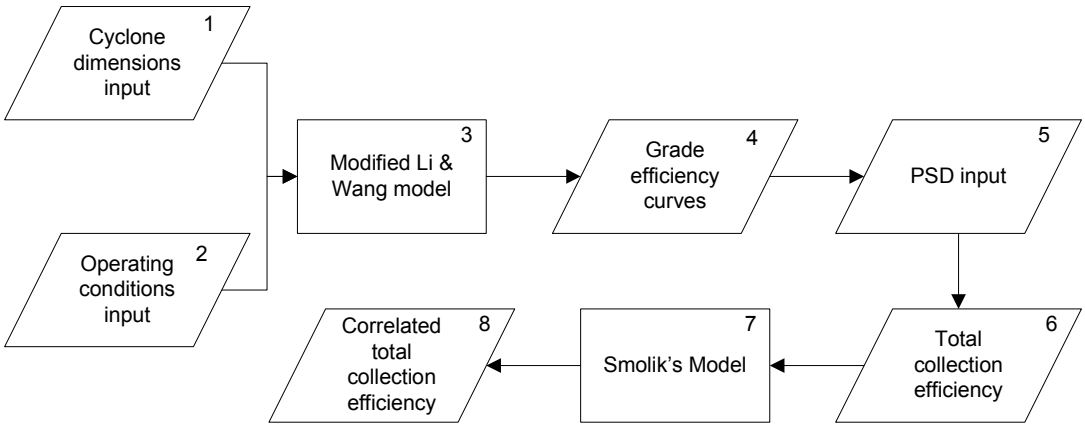

Figure 29: Li and Wang model methodology with Smolik's model

Figure 30 illustrates an example of use of the grade efficiency curves to obtain total collection efficiency values. There are two grade efficiency curves indicated by 81.15% and 64.34%. For illustration purposes, the 81.15% curve is more efficient because at lower particle diameters (x-axis) it delivers higher efficiencies (left-hand side of y-axis) than the 64.34% curve. The PSD shows the abundance or fraction (right-hand side of y-axis) of a certain size particle. In order to test a PSD

curve, the integral of such a PSD must deliver 100%, which means that the full spectrum of particles is represented by the curve. The legend in Figure 30 shows the resultant percentage of the PSD multiplied with the grade efficiency curve (represented by a solid line) to yield the total collection efficiency of 81.15%. The same was done for 64.34% (represented by a dotted line). To simplify, the lower the PSD curve is below the grade efficiency curve, the better the efficiency that will be obtained. Therefore, in Figure 30 the 81.15% curve is more efficient, as it covers more of the PSD curve. The calculated area below the grade efficiency curve and PSD curve is the total collection efficiency.

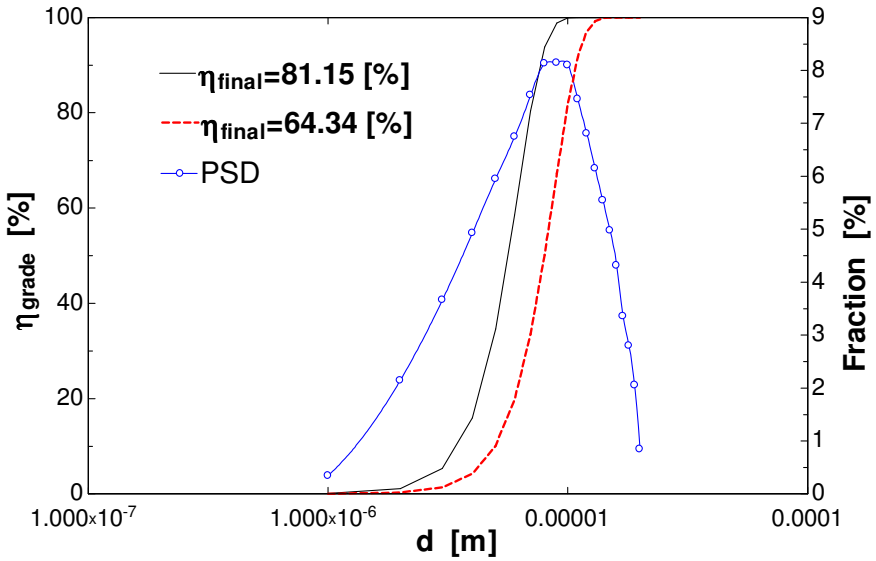

Figure 30: Grade efficiency curves and particle size distribution illustration

3.4 Model verification

In order to check the modified Li and Wang model, it was codified using Engineering Equation Solver (EES). The codified model was used to calculate different grade efficiencies of some known experiments and the model results were compared to the empirical data of these known experiments. The modified Li and Wang model is compared in this section with the Dirgo and Leith data (1985, comparison of experimental results with theoretical predictions). Dirgo and Leith conducted their experiments with a low particle concentration of approximately 50 mg/m³, so that the particles would have few agglomeration effects on each other. In Figure 31, Figure 32 and Figure 33 below, the experimental data was plotted with finite dots and the model output was plotted with a curve.

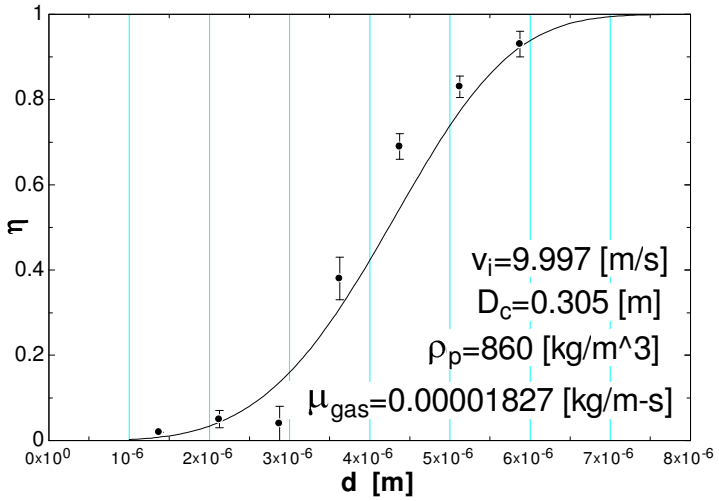

Figure 31: Stairmand high-efficiency cyclone separator with inlet 10 m/s (Dirgo & Leith, 1985)

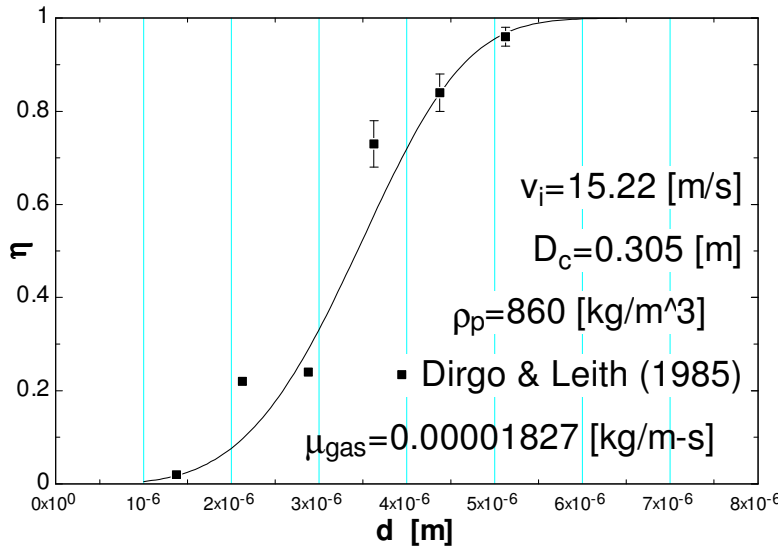

Figure 32: Stairmand high-efficiency cyclone separator with inlet 15 m/s (Dirgo & Leith, 1985)

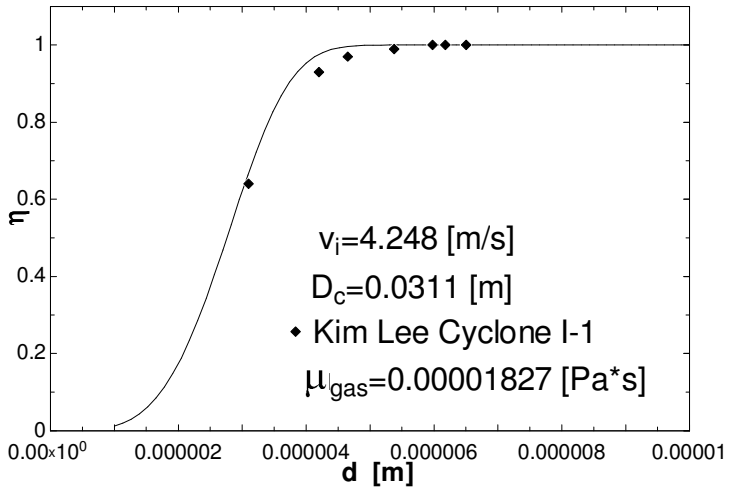

Figure 33: Kim and Lee's data of a very small cyclone (Kim & Lee, 1990:1007)

After the model demonstrated good correlation between three known experimental data, it was used to calculate the current ACF cyclone's total collection efficiency. The experimental data obtained from the ACF determined that the total collection efficiency was 60.2%. A PSD was discretised from the data and assumed to be measured just before the cyclone inlet.

Using the modified Li and Wang model on the ACF cyclone (with the input data as described above) resulted in a total collection efficiency of 66.2%. This result differs from the measured 60.2%, because the modified Li and Wang model excludes particle-loading concentration and the effect of the bottom diameter B_c on the collection efficiency. When Smolik's model was applied, the collection efficiency increased to 78%. Therefore, it can be assumed that there is little or no agglomeration of soot particles within the cyclone. According to Xiang et al. (2001) their documented experimental results (see Section 2.4.4) indicated that a larger B_c would decrease the efficiency.

3.5 Engineering Equation Solver

The following sections elaborate on the EES program interfacing and implementation. The basic user interface, input tables and output tables are explained in these sections. Engineering Equation Solver was used to calculate and represent the results graphically.

3.5.1 Graphical user interface

Figure 34 shows the graphical user interface (GUI) that allows the user to enter the cyclone's dimensions and operating conditions required by the model. This allows the user to determine quickly which parameters can be changed to obtain a more efficient design. The input and output data can be saved in tables that can be used to save certain cyclone design dimensions and test new design parameters that can assist in computer-aided design of CSs. Using this input table, the user can roughly verify a new CS design in minutes. The source code for this model will be given in the Appendix.

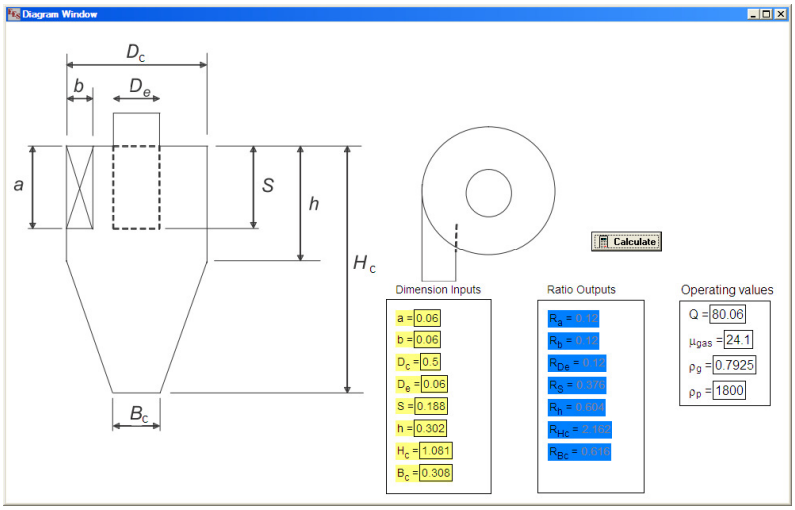

Figure 34: Engineering Equation Solver graphical user interface

3.5.2 Input tables

The tables shown in Figure 35 present the required input values required to satisfy the model methodology as shown by blocks 1, 2 and 5 in Figure 29. The dimensional data shown in Figure 35 is that of the current ACF cyclone. The geometric values and process conditions (such as those shown in Table 4 and Table 5, respectively) are used as input into the corresponding look-up tables as demonstrated in Figure 35. The PSD input is seen in Figure 36, in which *d* (column 1) is the particle diameter and $f_{fraction}$ (column 2) is the fraction of that specific particle size. By changing the values in these tables, predictions can be made for those specific parameters, for example changing the inlet

width to see the effect of that parameter on the performance of the CS. The predicted results will be discussed in the next chapter.

Cyclone Dimensions | Operating Values | Old cyclone ACF | Short | Long | Small | PSD-Discrete V1

Paste Special	1 a [m]	2 b [m]	3 B_c [m]	4 D_c [m]	5 D_e [m]	6 h [m]	7 H_c [m]	8 S [m]
Row 1	0.04638	0.04638	0.308	0.492	0.07366	0.302	1.081	0.188

Figure 35: Input table

3.5.3 Output tables

The EES model will have an output as shown in Figure 36. The PSD input is represented by the first two columns. The grade efficiency is calculated with the modified Li and Wang model. The fraction efficiency is obtained when $f_{fraction}$ (column 2) and η_{grade} (column 3) in the figure are multiplied. The sum of the fraction efficiency will result in the final efficiency (row 20, column 5) for that cyclone, according to the modified Li and Wang model. The grade efficiency in column 3 is used to plot the grade efficiency curves as shown in Figure 30.

Table 1

Multiply =

1..20	1 d [m]	2 $F_{fraction}$ [%]	3 η_{grade} [%]	4 $\eta_{fraction}$ [%]	5 η_{final} [%]	6 v_i [m/s]	7 L [m]	8 K
Run 1	1.000E-06	0.345	0.0001934	0.00006674	0.0001934	10.34	0.8179	0.000003065
Run 2	0.000002	2.142	0.003091	0.00662	0.002689	10.34	0.8179	0.00001226
Run 3	0.000003	3.664	0.01555	0.05697	0.01035	10.34	0.8179	0.00002759
Run 4	0.000004	4.928	0.04832	0.2381	0.02724	10.34	0.8179	0.00004904
Run 5	0.000005	5.95	0.1139	0.6776	0.05751	10.34	0.8179	0.00007663
Run 6	0.000006	6.747	0.2218	1.496	0.1041	10.34	0.8179	0.0001103
Run 7	0.000007	7.534	0.3716	2.799	0.1685	10.34	0.8179	0.0001502
Run 8	0.000008	8.129	0.5473	4.449	0.2465	10.34	0.8179	0.0001962
Run 9	0.000009	8.146	0.719	5.857	0.3274	10.34	0.8179	0.0002483
Run 10	0.00001	8.103	0.8555	6.932	0.4043	10.34	0.8179	0.0003065
Run 11	0.000011	7.46	0.9411	7.021	0.4677	10.34	0.8179	0.0003709
Run 12	0.000012	6.807	0.9819	6.684	0.5177	10.34	0.8179	0.0004414
Run 13	0.000013	6.148	0.996	6.124	0.5564	10.34	0.8179	0.000518
Run 14	0.000014	5.544	0.9994	5.541	0.5864	10.34	0.8179	0.0006008
Run 15	0.000015	4.977	0.9999	4.977	0.6102	10.34	0.8179	0.0006897
Run 16	0.000016	4.317	1	4.317	0.6287	10.34	0.8179	0.0007847
Run 17	0.000017	3.357	1	3.357	0.6419	10.34	0.8179	0.0008859
Run 18	0.000018	2.798	1	2.798	0.6522	10.34	0.8179	0.0009931
Run 19	0.000019	2.056	1	2.056	0.6595	10.34	0.8179	0.001107
Run 20	0.00002	0.848	1	0.848	0.6623	10.34	0.8179	0.001226

Figure 36: PSD input and output table

3.6 Chapter summary

Chapter 3 has explained the methodology behind the model used to calculate the predicted efficiency of the newly designed CS. The data that was used for deriving this model has been discussed in this chapter, and the implementation of this model in order to predict collection efficiencies has been described. The Li and Wang model has been described, its limitations noted and modification explained. The model was calibrated using the data received from the ACF and previous experimental data (given in the Appendix). The GUI of the model has been explained to indicate the user-friendliness thereof and to illustrate its use in the design of CSs.

CHAPTER 4: RESULTS

4.1 Introduction

This chapter discusses the predictions made using the modified Li and Wang model. The results of the comparison between the efficiencies of three cyclones and that of the current ACF CS are also reported here.

4.2 New cyclone designs

The newly proposed cyclone designs are depicted in Figure 37 to Figure 39. These cyclones are referred to as the *short cyclone, long cyclone* and *small cyclone*, respectively. The short cyclone has all the same geometries as the long cyclone except for h and H_c. The small cyclone has unique dimensions compared to the other two in every way except for the value of B_c. Table 6 gives the exact dimensions used and Figure 37 to Figure 39 indicates the corresponding position of each dimension. Figure 40 displays each cyclone's size with the same scale to provide a better perspective of their sizes relative to each other.

The cyclones were designed with what is commonly referred to as a wrap-around or spiral inlet design similar to that shown in Figure 13 (c). The wrap-around inlet converges within 180° into the cyclone, from which it continues to converge another 180° inside the cyclone as seen in Figure 37 to Figure 39. The short and long cyclones were designed with interchangeable cone sections. This enhanced empirical testing as five different cyclones resulted from this. The inlets were placed at an angle of about 10° and are rectangular, except for that of the small cyclone that uses a square inlet. The diameters D_e, D_c and B_c were measured from the inside of the CS (excluding the wall thickness) as well as with dimensions a and b. The other dimensions are self-explanatory and represented in Table 6, in which the newly designed cyclone dimensions are compared to those of the ACF cyclone.

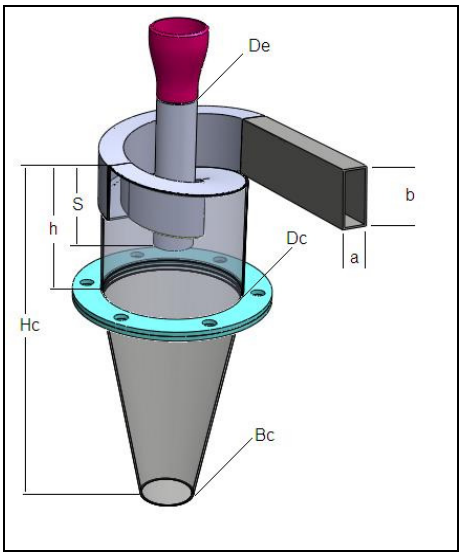

Figure 37: Short cyclone

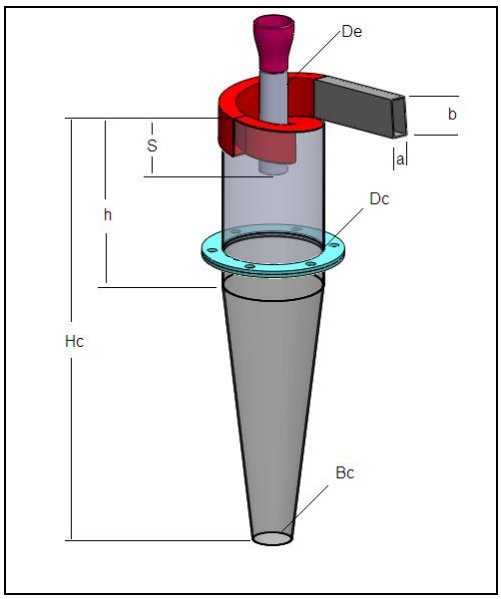

Figure 38: Long cyclone

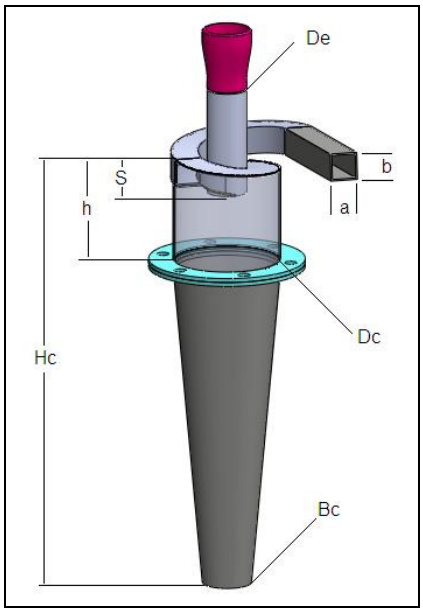

Figure 39: Small cyclone

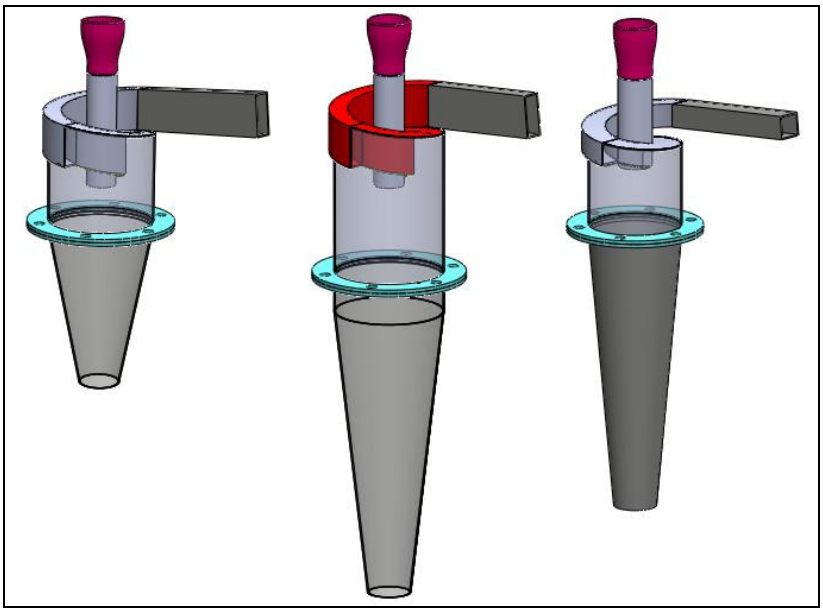

Figure 40: Short, long and small cyclones relative to each other

Table 6: Dimensions of the new cyclones

Dimensions (mm)	Short	Long	Small	Previous ACF
a	56	56	30	46.38
b	22	22	30	46.38
D_e	35	35	41	73.66
D_c	148	148	127	492
B_c	*56*	*56*	*56*	308
S	98	98	43	188
h	***154***	***225***	129	302
H_c	***398***	***680***	537	1081

The dimensions given in bold for the short and long cyclones indicate the only difference in lengths, while the underlined diameters for the short, long and small cyclones indicates the similarities between the designs. Table 7 presents the dimensions relative to the cyclones' body diameters D_c, in comparison to the Stairmand and Swift high efficiency data obtained from Fayed and Otten (1984:733; given in the Table 1). Figure 5 and Figure 37 indicate the dimension locations on a cyclone. Table 7 demonstrates that the long cyclone has similarities to the Stairmand high efficiency cyclone, except for a large difference in the ratio of D_e / D_c. The small cyclone and ACF cyclone have unique dimensions compared to other designs.

Table 7: Cyclone dimensions relative to body diameter

Ratios	Stairmand high efficiency	Swift high efficiency	Short	Long	Small	ACF
D_c	1.00	1.00	1.00	1.00	1.00	1.00
a / D_c	0.50	0.44	0.38	0.38	0.24	0.094
b / D_c	0.20	0.21	0.15	0.15	0.24	0.094
D_e / D_c	0.50	0.40	0.24	0.24	0.32	0.15
S / D_c	0.50	0.50	0.66	0.66	0.34	0.38
h / D_c	1.50	1.40	1.04	1.52	1.02	0.61
H_c / D_c	4.00	3.90	2.69	4.59	4.23	2.19
B_c / D_c	0.38	0.40	0.38	0.38	0.44	**0.63**

4.3 Predicted results of the newly designed cyclones

The results obtained with the Li and Wang model are represented in these sections. This includes the calculated collection efficiency of each cyclone for a particle re-entrainment of zero and 0.5. The pressure drop is calculated as well.

4.3.1 Collection efficiency

The data discussed in Sections 3.2.2 (operating parameters) and 3.2.3 (PSD) was used to determine the following results with the new CS dimensions, as tabulated in Table 6. Owing to the limitations of the selected model (Li and Wang's model) the short and long cyclones have similar predicted efficiencies (this was explained in Section 3.3.2). The model does not use the total cyclone height as a factor for calculating the efficiency. The short and long cyclones, which have the same top geometry (inlet, outlet, diameter and so on) but different cone lengths, have the same predictions. Therefore, these two cyclones are discussed together.

During the simulation comparison between the long/short and small cyclone, some uncertainty as to the re-entrainment condition existed. It was therefore decided that for both cyclones, the simulation should be run without the effect of re-entrainment and with re-entrainment set at α=0. Therefore, if α is larger, the efficiency will decrease. This assumption was used by Li and Wang (1989:668).

Figure 41 shows a comparison between the different grade efficiencies of the previous and newly designed cyclones. Figure 42 and Figure 43 present the results of the calculated grade efficiency with both re-entrainment conditions for the relevant dimensions of the long/short and small cyclones. An inlet gas velocity of 18.05 m/s was calculated. When it was assumed that no particles would bounce (thus re-entrainment was disregarded; $\alpha = 0$), the efficiency was calculated as 95.56% (indicated by the solid line). When a conservative re-entrainment was assumed, the efficiency decreased to 93.24%. Figure 43 shows the results of the small cyclone and as before, the solid line represents zero re-entrainment and the dotted line indicates $\alpha = 0.5$. Note that there is a small overshoot when the grade efficiency reaches 100% due to the polynomial fit of the data points. The model showed a predicted efficiency of 98.18% and when a conservative re-entrainment was included the efficiency decreased to 97.2%. It can be seen that in both re-entrainment cases, the small cyclone has a higher efficiency, approximately 3.5%, that the long/short version.

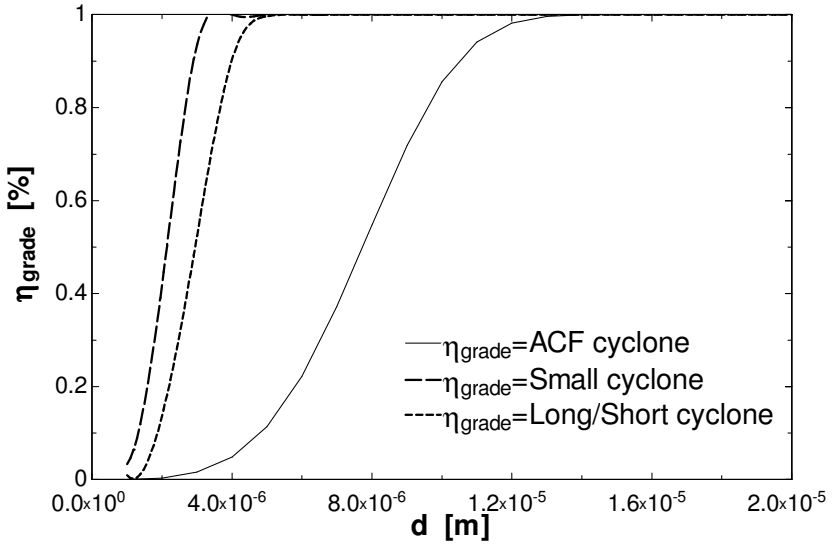

Figure 41: Grade efficiency comparison between ACF, small and short/long cyclones

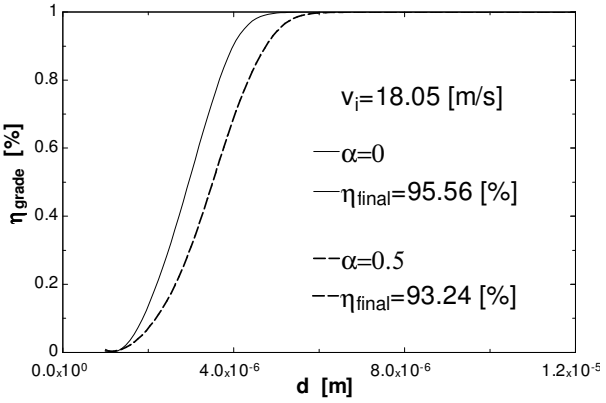

Figure 42: Short/long cyclone predictions

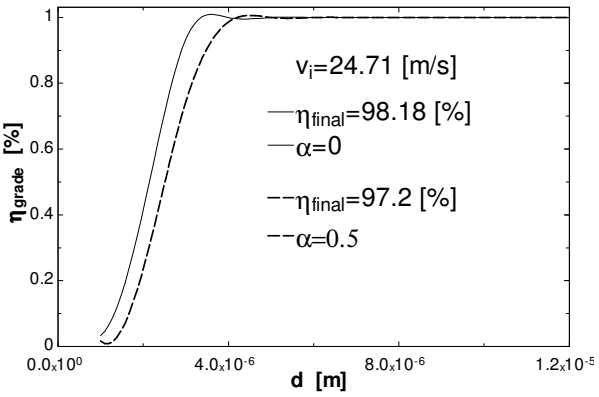

Figure 43: Small cyclone predictions

4.3.2 The pressure drop of the cyclones

The pressure drop was calculated using equations (2.3.5.1) and (2.3.5.2). The results obtained are represented in Table 8. The small cyclone showed the smallest pressure drop followed by the long cyclone and then the short cyclone. The code for these calculations will be given in the Appendix.

Table 8: Pressure drop

	Small CS	Long CS	Short CS
ΔP (Pa)	1454	1623	2201
ΔH	6.032	12.68	17.2

4.4 Chapter summary

In this project, the modified Li and Wang model was used to predict the collection efficiencies of the newly designed CSs. This chapter has depicted the results of these predictions graphically. The collection efficiency of the short/long cyclone was predicted as 95.56%, while the small cyclone was predicted as 98.18%, with zero particle re-entrainment. The efficiencies dropped to 93.24% and 97.2%, respectively, owing to the introduction of particle re-entrainment. The small cyclone had the smallest pressure drop of 1454 Pa, while the long cyclone had a pressure drop of 1623 Pa and the short cyclone had a pressure drop of 2201 Pa. The conclusions drawn from the results that have been presented in this chapter will be discussed in the next chapter.

CHAPTER 5: CONCLUSIONS

5.1 Introduction

This chapter elaborates on the results presented in Chapter 4 and provides an interpretation of the grade efficiency graphs given in Chapter 4. By employing the numerical model and interpreting the results correctly, the designers of the new cyclones could improve/substantiate these designs and make relevant suggestions. The numerical model could be used to predict the influence of various parameters on the grade efficiency of different cyclone designs, given the limitations as previously mentioned. Conclusions made from the literature study will also be discussed in this chapter.

5.2 Cyclones predictions

The predictions calculated are used to conclude on the implications that certain design parameters have on the performance of a CS. Such an implication, for example, is the manner in which the inlet area or cyclone body diameter will affect the collection efficiency of a CS. As noted, the collection efficiency difference between the new designs is fairly small, approximately 4%. This questions the accuracy of the modified Li and Wang model due to its simplifications. This uncertainty can only be resolved by empirical testing.

5.2.1 Cyclones collection efficiencies

As shown in Figure 42 and Figure 43, the model results predict that the small cyclone has the best efficiency (98%) in comparison to the efficiency of the short/long cyclone (95%). When comparing physical parameters between these cyclones, it is clear that the small cyclone has a smaller body diameter D_c and inlet area $a \times b$. Firstly, according to the modified Li and Wang model, if D_c is decreased and all other parameters remain the same, efficiency will increase. In order to verify this, the body diameter of the short/long CS was changed from $D_c = 0.148\,\text{m}$ to $D_c = 0.108\,\text{m}$, the result of which is given in Figure 44. In order to verify this phenomena, the particle radial velocity at the wall of the short/long CS in Figure 44 was calculated for $D_c = 0.148\,\text{m}$ and $D_c = 0.108\,\text{m}$ as $w_w = 5.813\,\text{rad/s}$ and $w_w = 7.967\,\text{rad/s}$, respectively. Therefore, the smaller diameter D_c is, the larger the particle radial velocity will be, and efficiency in turn will be increased. Secondly, if the inlet

area is reduced and the flow remains the same, the inlet velocity will increase. Figure 45 shows the results of reducing the inlet of the short/long cyclone to the same inlet size of the small cyclone. The effect of this was an increased inlet speed of approximately 18 m/s to 24 m/s, and the particle radial velocity according to the model was calculated as $w_w = 5.813$ and $w_w = 10.89$, respectively.

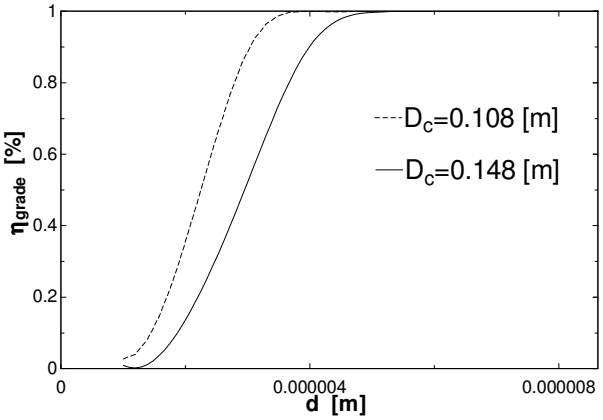

Figure 44: The effect of cyclone diameter

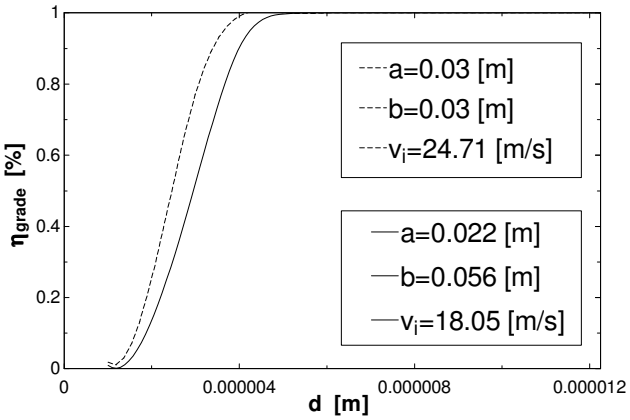

Figure 45: The effect of cyclone inlet area

Therefore, according to the modified Li and Wang model, the small cyclone has a better efficiency owing to smaller body diameter and smaller inlet size. Furthermore, the wrap-around design is expected to be an advantage as the design may reduce eddy currents that typically form with normal tangential inlets. Unfortunately, the theoretical model cannot predict the effect of this on the total collection efficiency of the cyclones.

5.2.2 Cyclones' angled inlets and dipleg sizes

All three newly designed cyclones have an angled inlet of approximately 10° from the horizontal offset. From the literature stated in Section 2.4.6, the greater the angle, the better the collection efficiency will be. Qian and Wub (2009:1) demonstrated that an increased angled inlet, which could be caused by the reduction of swirling flow at the inlet, reduces pressure drop. The poor efficiency of the ACF cyclone could be due to the large dipleg diameter (dust outlet) B_c. Xiang *et al.* (2001:560) conclude that the larger the dust outlet diameter is, the greater the loss on the collection efficiency will be.

5.2.3 Cyclones' cone lengths

The only difference between the long and short cyclones shown in Figure 38 and Figure 39, respectively, is their lengths h (height above the cone) and H_c (height of the cyclone). The modified Li and Wang model can't predict this effect, concluding from supporting literature it can be stated that the longer the cone the more efficient it will be (Avci & Karagoz, 2003:948–950). It was expected that the longer cone would be more efficient than the shorter cone, owing to the residence time of the particles inside the cone. The longer the residence time is, the greater the time will be for the particles to move to the wall of the CS and into the hopper. The larger the cyclone cone length is (with similar outlet sizes and diameters), the steeper the cone gradient (the angle measured relative to the horizontal plane) will be. From a gravitational point of view, the steeper the gradient is, the easier it will be for particles that hit the cyclone wall owing to the centrifugal action to fall down into the CS and prevent clogging of particles on the CS wall. This is demonstrated in Figure 46.

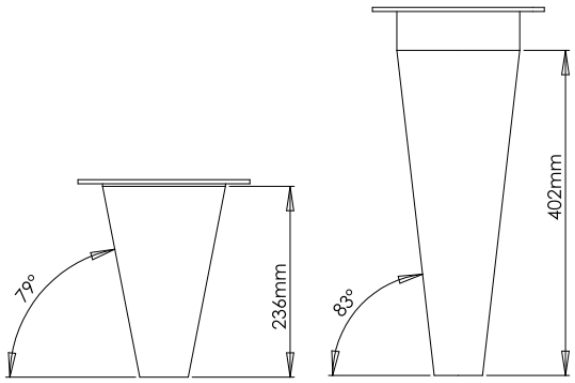

Figure 46: Cone angle

5.2.4 Agglomeration

As noted in Section 3.4 (see also the Appendix), the ACF cyclone had an initial efficiency of approximately 60.2% that was measured empirically with an unknown error margin. The calculated value was 66.23% and was assumed to be at a load particle concentration of 10 g/m³. Smolik's model adjusted the new efficiency to approximately 78% for a concentration load of 121.6 g/m³. Therefore, it could be concluded that either the soot particles do not agglomerate or they do so in such a way that it is not evident. However, as previously mentioned a large dimension B_c has a negative effect on the

total collection efficiency and the ACF cyclone has a very large B_c diameter. Owing to this uncertainty, it cannot be concluded that no agglomeration occurs.

The ACF cyclone had an inlet velocity of approximately 10 m/s compared to the 18 m/s and 24.7 m/s of the short/long and the small cyclones. As previously mentioned, the inter-particle force (the van der Waals forces) between the soot particles is unknown. There is a chance that the particles can de-agglomerate at higher velocities, which will reduce the particles' average size and thereby decrease the total collection efficiency.

5.2.5 Pressure drop

Table 8 indicated that the small cyclone has the lowest pressure loss. According to equation (2.3.5.1), a higher inlet velocity will directly increase the pressure drop over a CS. The model calculations demonstrated that the small cyclone has the highest inlet velocity. This may appear contradictory at first, but upon inspecting the dimensions of the small cyclone design it is evident that the diameter D_e is larger than the other designs (see Table 7). Equation (2.3.5.2) demonstrates that if D_e is increased, the pressure loss will decrease hyperbolically. For this reason, the small cyclone has the lowest pressure drop of 1.454 kPa compared to that of the long cyclone of 1.623 kPa and that of the short cyclone of 2.201 kPa. The pressure drop of the long and short cyclones differs because of their dimension differences h and H_c. If these dimensions were lengthened, then according to equation (2.3.5.2) the pressure drop would decrease.

5.3 Chapter summary

According to the modified Li and Wang model, the best collection efficiency will be achieved by the small cyclone. The small cyclone achieves this superior efficiency because of a smaller cyclone body diameter D_c and a smaller inlet area. Changes to these dimensions would increase the particle radial velocity. The particle radial velocity for the short/long CS was calculated slower than compared to the small CS. Therefore, the particles in the small cyclone will experience larger centrifugal force and be removed more effectively. It was expected that the wrap-around inlet design would improve the performance of the cyclone; however, this assumption could not be proved with the modified Li and Wang model. According to Qian and Wub's experiments, the angled inlet would have a positive effect

on the collection efficiency and pressure drop. The small cyclone has the lowest pressure drop amongst the CSs investigated. This is due to a larger gas outlet diameter D_e. Unfortunately, the effect of soot agglomeration could not be verified in this project, as a series of experiments with different types of particles at different inlet speeds are needed to identify agglomeration. However, this project required only that the new designs perform according to the predicted values. Should the newly designed cyclones deliver the same collection efficiency as the ACF cyclone of 60.2%, it would be regarded as beneficial because of the SG design of these new cyclones. Even if the new cyclones don't outperform the ACF cyclone, they have the advantage of being a SG design and that will make them worth while from a nuclear criticality safety point of view. The next chapter will present recommendations that can improve CS performance and suggest future CS development.

CHAPTER 6: RECOMMENDATIONS

6.1 Introduction

This chapter discusses future research that can be done to improve the CS designs and to improve understanding of their operation. This mini-dissertation presented a literature review that identified new techniques and shortcomings of CS, as well as techniques for modelling cyclones. Recommendations are made that can improve the CS designs, should the experimental results not correlate with the results predicted in this project.

6.2 Improvements on the three new designs

These sections introduce modifications that can be used to enhance the performance of a CS. These include the effects that the inlet velocity will have on the performance of a CS and the manner in which to address these issues. Recommendations of different cone bottom combinations are discussed, as well as the design of different angle inlets. Also, methods for reducing the pressure drop over a CS are examined.

6.2.1 Inlet velocity

According to theory, the higher the inlet velocity in a CS, the better the collection efficiency will be. There are three disadvantages related to a higher inlet velocity. Firstly, the particles can de-agglomerate, making them smaller and harder to be collected. Secondly, the inlet velocity increases the turbulent diffusion coefficient, which will reduce the collection efficiency owing to a weaker vortex. Therefore, at very high inlet speeds a noticeable decline in the collection efficiency will be observed. Lastly, the higher the inlet velocity, the higher the pressure drop will be over the CS. With this in mind, a CS will perform at its best at an optimum speed. Should the collection efficiency not be what is expected, dimensional alterations to the inlet can be made. These alterations should preferably be made to the a dimension instead of the b dimension, as the latter will decrease the vortex component and more particles will be able to slip out of the CS via the eddy currents. Therefore, the inlet size can be optimised empirically.

6.2.2 Cone geometry

As predicted, the small cyclone will have the better collection efficiency, owing to its smaller body design and smaller inlet. The gas outlet of the small cyclone can be reduced should the efficiency be lower than expected. If this cyclone does not perform well, owing to the higher inlet speed mentioned above, then the short and long cyclones would need to be used instead. According to the cone shape or the angle that the cone makes, as shown in Figure 46, the long cyclone's cone will be the best suited for particle removal. Therefore, it would be beneficial to use the small cyclone's top with the long cyclone's bottom, because the steeper the cone's slope, the better the collection efficiency will be.

6.2.3 Angled inlets

The angles of the new CS designs could be increased to the suggested angle of 45°, measured from the horizontal plane. This will increase the collection efficiency and lower the pressure drop. As the residence time of the soot particles inside the cyclone plays a major role in collection efficiency, an angled inlet of greater than 45° is not recommended. Should the inlet angle be too large, the soot will have less time to be removed by centrifugal force. An angle that is too large will reduce the collection efficiency, particularly for the small particles.

6.2.4 Pressure drop decrease

As previously mentioned, the small cyclone has the lowest pressure loss because of its larger gas outlet (vortex finder) diameter. This can also be applied to the other two cyclones, should pressure loss be a significant concern. An increment in the inlet angle will lower the pressure drop and enlarge the dust outlet diameter B_c or gas outlet D_e. All these methods lower the pressure drop without the need to change operating conditions, such as flow rate.

6.3 External optimisation

The term *external optimisation* refers to a method or an attachment that can be added to a CS without physically changing the core components or structure of a CS. The ACF uses different flow rates during operation where each coating layer in the CVD process has its own flow rate. The new cyclones were designed and modelled for the inner and outer PyC layers' flow rates that are

approximately 80 m³/h. The porous carbon layer has a flow rate of approximately half that of the other two layers. This can dramatically decrease the collection efficiency, as shown in Figure 47. In order to solve this problem, an external flow can be injected. This can be compressed air injected 180° opposite to the dust inlet. If the slower flow rate is 35 m³/h, then the injected compressed air should be 45 m³/h to achieve the optimal designed flow rate of 80 m³/h.

Should the new cyclone be fitted but not perform well and financial constraints prevent a design of a new CS, then a PoC attachment (Section 2.5.1) can be investigated as a possible solution. The PoC can be used as a pre-cyclone for the next cyclone fitted in series; this will increase the collection efficiency of that cyclone owing to agglomeration of soot and removal of soot with the swirl present at the gas outlet.

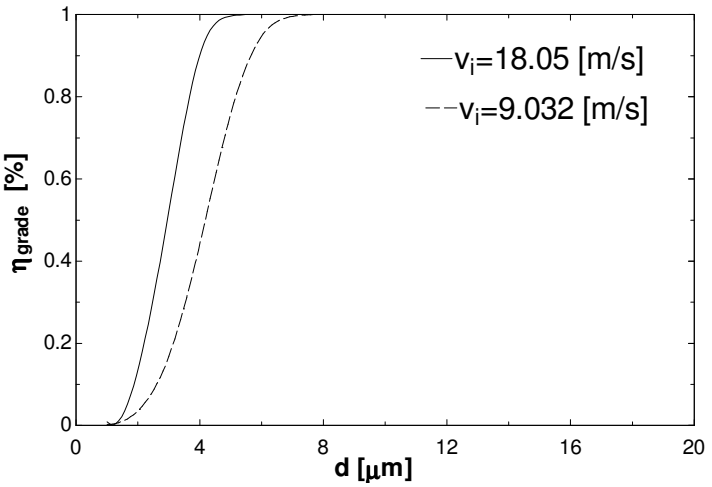

Figure 47: Slower inlet speed for long cyclone

6.4 Recommendations for future research

Collection efficiency models should incorporate particle agglomeration in order to enhance their prediction accuracy. The particle agglomeration model should account for different types of particles in order to distinguish, for example, between fly ash and cement. The influence of the wrap-around inlet should be tested and compared to a normal angled inlet. The results should be analysed in order to determine whether the wrap-around design is worth the higher capital cost of building and designing a wrap-around inlet.

The collection efficiency and the pressure loss models should incorporate new inlet designs such as the wrap-around design. Future development and verification should be conducted on models that include all the dimensions of a CS, until a reliable universal model is available. This will enhance design techniques for future CSs that can achieve near 100% efficiency and reduce the risk of small-particle inhalation. The effect of a CS used for removing diesel soot in boats, cars, trucks and so on could also be investigated. Such a CS would reduce the amount of black smoke released into the atmosphere and the effect of global warming.

6.5 Chapter summary

This chapter can be summarised as different techniques and conditions that can improve the performance of CSs and recommendations that can enhance the development of CSs. For example, the inlet speed should be optimised for specific particles or agglomerates and different CS designs. The small CSs efficiency can be improved by reducing the gas outlet diameter. The CS inlet angle should be increased in order to find an optimal degree that will enhance the CSs performance. The external flow input should be investigated, as it will be a suitable optimiser for a CS that operates at different flow rates within the CVD process.

The proposed CSs, according to the data supplied and the data calculated by the model used, will be a successful replacement for current ACF CS.

LIST OF SYMBOLS

a = cyclone inlet height (m)

b = cyclone inlet width (m)

B_c = cyclone dust outlet (m)

c = particle concentration (g/m³)

c_0, c_1 = inlet and outlet concentration of particles (g/m³)

d = particle diameter (m)

D_c = cyclone body diameter (m)

D_e = cyclone gas outlet diameter (m)

$d_{p50\%}$ = particle diameter that will have 50% collection efficiency (m)

f = friction coefficient

h = cyclone cylinder height (height above the cone) (m)

H_c = cyclone height (m)

K = constant correlating cyclone structure and flow condition

L = natural length of cyclone (Alexander) (m)

n = cyclone vortex exponent

N_e = number of effective turns the gas makes within the cyclone

Q = volumetric gas flow rate (m³/s)

R_c = radius $(D_c - D_e)$ (m)

r_w, r_n = radial dimension (m)

S = cyclone gas outlet duct length (vortex finder length) (m)

T = absolute temperature (K)

u = tangential component of gas velocity in the cyclone vortex (m/s)

V_i = inlet gas velocity (m/s)

w = radial particle velocity (rad/s)

Greek letters

α = particle bounce or re-entrainment coefficient

λ = characteristic value

θ = angular coordinate

η = collection efficiency (%)

η_j = fraction efficiency (%)

ρ_p = particle mass density (kg/m³)

ρ_g = gas density (kg/m³)

μ = gas viscosity (m²/s)

APPENDIX

A.1 Program code

The programming code is given in the following sections. These sections include the source code for the EES model and the formatted equations.

A.1.1 Engineering Equation Solver code for calculation of Advance Coater Facility cyclone

```
"Input cyclone dimensions  from the lookup table:"
a=Lookup('Cyclone Dimensions', 1, 'a')                    "See Figure 5 for  dimension inputs"
b=Lookup('Cyclone Dimensions', 1, 'b')
D_e=Lookup('Cyclone Dimensions', 1, 'D_e')
D_c=Lookup('Cyclone Dimensions', 1, 'D_c')
S=Lookup('Cyclone Dimensions', 1, 'S')
h=Lookup('Cyclone Dimensions', 1, 'h')
H_c=Lookup('Cyclone Dimensions', 1, 'H_c')                "Note that model does not use the height of the cyclone as input unless the natural length > actual length"
B_c=Lookup('Cyclone Dimensions', 1, 'B_c')

"-------------------------------------------------Operating values-------------------------------------------------------------"
                                                          "As obtained from the ACF"
Q=Lookup('Operating Values',1,'Q')                        "Process gas flow rate per hour"
mu_gas=Lookup('Operating Values',1,'mu_gas')              "Viscosity of process gases"
rho_gas=Lookup('Operating Values',1,'rho_gas')            "Density of process gases"
T=333                                                     "60℃"
rho_particle=Lookup('Operating Values',1,'rho_particle')  "Assumed particle density of soot 1800 kg/m^3"

"-------------------------------------------------Calculations on inputs-------------------------------------------------------"
Q_s=Q/3600                                                "Calculates the flow rate per second"
v_i=Q_s/(a*b)                                             "The inlet speed: the model is only dependant on the inlet speed and value b; therefore, it is independent from the true hydraulic diameter, for example a circle can be approximated with a square as long as their areas are the same"
nu_gas=mu_gas/rho_gas                                     "The dynamic viscosity"
r_w=D_c/2                                                 "Radial dimension of cyclone body diameter"
r_n=D_e/2                                                 "Radial dimension of vortex finder diameter"

Re= (rho_gas*V_i*b)/mu_gas                                "Reynolds number. If Re>3000 it is assumed turbulent (Avci & Karagoz, 2003:9), but large cyclones in general are turbulent (small cyclone is approximately 5 cm and large is approximately 15 to 30 cm)"

"-------------------------------------------------Assumptions------------------------------------------------------------------"
//alpha=0.235                                             "Particle bounce or re-entrainment coefficient"
alpha=0                                                   "Between 0 and 0.5 from Li and Wang, 0.5 is most
    conservative 0.238, correlates model with experimental results"
```

```
//alpha=0.328                                   "Value to calibrate the collection efficiency of ACF to
60.2%"
//alpha=0.5                                     "Conservative"
u=v_i                                           "Tangential component of gas velocity in cyclone
                                                vortex assumed equal to the inlet velocity"

f=0.02                                          "Assumed friction coefficient Dirgo & Leith (1985;
                                                quoted by Li and Wang, 1989 )"

"---------------------------------------------------- Li and Wang model----------------------------------------------"

eta_grade=1-exp(-lambda*theta_1)                "Grade efficiency according to Li and Wang"
theta_1=2*pi*(S+L)/a                            "Angular coordinate"

L=2.3*D_e*(D_c^2/(a*b))^(1/3)                   "Natural length from Li and Wang (Alexander, 1949)
                                                if natural length < actual length"
//L=H_c-S                                       "If natural length > actual length, use the length of
                                                the cyclone"

lambda=((1-alpha)*K*w_w)/(D_r*r_w^n)            "Parameter lambda"
K=  ((1-n)*(rho_particle-rho_gas)*(d)^2*Q_s)  /  (18*nu_gas*b*(r_w^(1-n)-r_n^(1-n))) "Parameter K"
w_w=((rho_particle-rho_gas)*u^2*(d)^2)/(18*nu_gas*r_w) "Radial particle velocity at wall"

D_r=0.052*R_c*u*sqrt(f/8)                       "Turbulent diffusion coefficient from Taylor (1954;
                                                quoted by Li and Wang, 1989 )"

R_c=(D_c-D_e)/2                                 "Radius dimension between cyclone diameter and
vortex outlet"

//n=1-((1-0.67*D_c^0.14)*(T/283)^0.3)           "Vortex exponent from Li and Wang"
n=1-((1-0.5*D_c^0.14)*(T/283)^0.3)              "Vortex exponent modified, as proposed by Gimbun
                                                et al. (2004:43)"

eta_fraction=eta_grade*F_fraction               "Using the PSD to calculate the fraction of the total
efficiency"
eta_final=SUMPARAMETRIC('Table 1', 'eta_fraction')/SUMPARAMETRIC('Table 1', 'F_fraction') "Total
efficiency is the sum of these fractions calculated above"


"----------------------------------------------------Smolik's model-------------------------------------------------"
C_1=10                                          "g/m^3"
C_2=121.6                                       "g/m^3"
eta_final_concentration=1-(1-eta_final)*(C_1/C_2)^0.18  "Smolik's correlation (see Section 2.3.3)"
```

A.1.2 Formatted Engineering Equation Solver code for calculation of Advance Coater Facility previous cyclone

Input cyclone dimensions from the lookup table:

a = **Lookup** ['Cyclone Dimensions', 1, 'a'] *See Figure 5 for dimension inputs*

b = **Lookup** ['Cyclone Dimensions', 1, 'b']

D_e = **Lookup** ['Cyclone Dimensions', 1, 'D_e']

D_c = **Lookup** ['Cyclone Dimensions', 1, 'D_c']

S = **Lookup** ['Cyclone Dimensions', 1, 'S']

h = **Lookup** ['Cyclone Dimensions', 1, 'h']

H_c = **Lookup** ['Cyclone Dimensions', 1, 'H_c'] *Note that model does not use the height of the cyclone as input unless the natural length > actual length*

B_c = **Lookup** ['Cyclone Dimensions', 1, 'B_c']

----------*Operating values*----------

As obtained from the ACF

Q = **Lookup** ['Operating Values', 1, 'Q'] *Process gas flow rate per hour*

μ_{gas} = **Lookup** ['Operating Values', 1, 'mu_{gas}'] *Viscosity of process gases*

ρ_{gas} = **Lookup** ['Operating Values', 1, 'rho_{gas}'] *Density of process gases*

T = 333 *60 ℃*

$\rho_{particle}$ = **Lookup** ['Operating Values', 1, '$rho_{particle}$'] *Assumed particle density of soot 1800 kg/m^3*

----------Calculations on inputs----------

$$Q_s = \frac{Q}{3600}$$ *Calculates the flow rate per second*

$$v_i = \frac{Q_s}{a \cdot b}$$ *The inlet speed: the model is only dependant on the inlet speed and value b; therefore, it is independent fror the true hydraulic diameter, for example a circle can be approximated with a square as long as thei areas are the same*

$$v_{gas} = \frac{\mu_{gas}}{\rho_{gas}}$$ *The dynamic viscosity*

$$r_w = \frac{D_c}{2}$$ *Radial dimension of cyclone body diameter*

$$r_n = \frac{D_e}{2}$$ *Radial dimension of vortex finder diameter*

$$Re = \frac{\rho_{gas} \cdot v_i \cdot b}{\mu_{gas}}$$

Reynolds number. If Re>3000 it is assumed turbulent (Avci & Karagoz, 2003:9), but large cyclones in general are turbulent (small cyclone is approximately 5 cm and large is approximately 15 to 30 cm)

----------Assumptions----------

$\alpha = 0$ *Between 0 and 0.5 from Li and Wang, 0.5 is most conservative 0.238, correlates model with experimental results*

$u = v_i$ *Tangential component of gas velocity in cyclone vortex assumed equal to the inlet velocity*

$f = 0.02$ *Assumed friction coefficient from Li and Wang (Dirgo & Leith, 1985)*

---------- Li and Wang model----------

$\eta_{grade} = 1 - \exp\left[-\lambda \cdot \theta_1\right]$ *Grade efficiency according to Li and Wang*

$\theta_1 = 2 \cdot \pi \cdot \left[\frac{S + L}{a}\right]$ *Angular coordinate*

$L = 2.3 \cdot D_e \cdot \left[\frac{D_c^{\,2}}{a \cdot b}\right]^{[1\ /\ 3]}$ *Natural length from Li and Wang (Alexander, 1949) if natural length < actual length*

$\lambda = \frac{[1 - \alpha] \cdot K \cdot w_w}{D_r \cdot r_w^{\,n}}$ *Parameter lambda*

$K = \frac{[(1 - n) \cdot (\rho_{particle} - \rho_{gas})] \cdot d^2 \cdot Q_s}{18 \cdot \nu_{gas} \cdot b \cdot [r_w^{(1 - n)} - r_n^{(1 - n)}]}$ *Parameter K*

$w_w = \frac{[\rho_{particle} - \rho_{gas}] \cdot u^2 \cdot d^2}{18 \cdot \nu_{gas} \cdot r_w}$ *Radial particle velocity at wall*

$D_r = 0.052 \cdot R_c \cdot u \cdot \sqrt{\frac{f}{8}}$ *Turbulent diffusion coefficient from Li and Wang (Taylor, 1954)*

$R_c = \frac{D_c - D_e}{2}$ *Radius dimension between cyclone diameter and vortex outlet*

$n = 1 - [1 - 0.5 \cdot D_c^{\,0.14}] \cdot \left[\frac{T}{283}\right]^{0.3}$ *Vortex exponent modified, as proposed by Gimbun et al. (2004:43)*

$\eta_{fraction} = \eta_{grade} \cdot F_{fraction}$ *Using the PSD to calculate the fraction of the total efficiency*

$\eta_{final} = \frac{\mathbf{SumParametric}\left['Table\ 1',\ 'eta_{fraction}'\right]}{\mathbf{SumParametric}\left['Table\ 1',\ 'F_{fraction}'\right]}$ *Total efficiency is the sum of these fractions calculated above*

----------Smolik's model----------

$C_1 = 10 \ g/m^3$

$C_2 = 121.6 \ g/m^3$

$\eta_{final,concentration} = 1 - [1 - \eta_{final}] \cdot \left[\frac{C_1}{C_2}\right]^{0.18}$ *Smolik's correlation*

A.2 Engineering Equation Solver pressure drop calculations

The pressure drops are calculated from the following equations:

$$\Delta H_{short} = 20 \cdot \frac{as \cdot bs}{D_{es}^{\ 2}} \cdot \left[\frac{\frac{Ss}{D_{cs}}}{\frac{H_{cs}}{D_{cs}} \cdot \frac{hs}{D_{cs}} \cdot \frac{B_{cs}}{D_{cs}}} \right]^{(1/3)}$$

$$\Delta H_{long} = 20 \cdot \frac{a \cdot b}{D_e^{\ 2}} \cdot \left[\frac{\frac{S}{D_c}}{\frac{H_c}{D_c} \cdot \frac{h}{D_c} \cdot \frac{B_c}{D_c}} \right]^{(1/3)}$$

$$\Delta H_{small} = 20 \cdot \frac{am \cdot bm}{D_{em}^{\ 2}} \cdot \left[\frac{\frac{Sm}{D_{cm}}}{\frac{H_{cm}}{D_{cm}} \cdot \frac{hm}{D_{cm}} \cdot \frac{B_{cm}}{D_{cm}}} \right]^{(1/3)}$$

$$\Delta H_{short} = \frac{2 \cdot \Delta P_{short}}{p_g \cdot v_{short}^{\ 2}}$$

$$\Delta H_{long} = \frac{2 \cdot \Delta P_{long}}{p_g \cdot v_{long}^{\ 2}}$$

$$\Delta H_{small} = \frac{2 \cdot \Delta P_{small}}{p_g \cdot v_{small}^{\ 2}}$$

REFERENCES

AVCI, A. & KARAGOZ, I. 2003. Effects of flow and geometrical parameters on the collection efficiency in cyclone separators. *Journal of Aerosol Science*, 34(7):937–955. Available: ScienceDirect.

BIKA, D.G., GENTZEL, M. & MICHAELS, J.N. 2001. Mechanical properties of agglomerates. *Powder Technology*, 117(1):98–112. Available at: ScienceDirect.

BOHNET, M. 1995. Influence of the gas temperature on the separation efficiency of aerocyclones. *Chemical Engineering and Processing*, 34(3):151–156. Available: ScienceDirect.

CHEN, J. & SHI, M. 2003. Analysis on cyclone collection efficiencies at high temperatures. *China Particuology*, 1(1):20–26. Available at: ScienceDirect.

CORTÉS, C. & GIL, A. 2007. Modeling the gas and particle flow inside cyclone separators. *Progress in Energy and Combustion Science*, 33(5):409–452. Available: ScienceDirect.

DIRGO, J. & LEITH, D. 1985. Cyclone collection efficiency: comparison of experimental results with theoretical predictions. *Aerosol Science and Technology*, 4(4):401–415. Available: Informaworld.

FAYED, M.E. & OTTEN, L. 1984. Handbook of Powder Science and Technology. New York: Van Nostrand. 850 p.

GIMBUN, J., CHOONG, T.S.Y., FAKHRU'L-RAZI, A. & CHUAH, T.G. 2004. Prediction of the effect of dimension, particle density, temperature, and inlet velocity on cyclone collection efficiency. *Jurnal Teknologi*, 40(F):37–50. Available at: ScienceDirect.

HONG, S., WOOLDRIDGE, M.S., IM, H.G., ASSIANIS, D.N. & PITSCH, H. 2005. Development and application of a comprehensive soot model for 3D CFD reacting flow studies in diesel engine. *Combustion and Flame*, 143(1–2):11–26. Available: ScienceDirect.

JI, Z., XIONG, Z., WU, X., CHEN, H. & WU, H. 2009. Experimental investigations on a cyclone separator performance at an extremely low particle concentration. *Powder Technology*, 191(3):254–259. Available: ScienceDirect.

JO, Y., TIEN, C. & RAY, M.B. 1999. Development of a post cyclone to improve the efficiency of reverse flow cyclones. *Powder Technology*, 113(2000):97–108. Available at: ScienceDirect.

KAYA, F. & KARAGOZ, I. 2009. Numerical investigation of performance characteristics of a cyclone prolonged with a dipleg. *Chemical Engineering Journal*, 151(1–3):39–45. Available: ScienceDirect.

KIM, J.C & LEE, K.W. 1990. Experimental study of particle collection by small cyclones. *Aerosol Science and Technology*, 12(4):1003–1015. Available: ScienceDirect.

LI, E. & WANG, Y. 1989. A new collection theory of cyclone separators. *AIChE Journal,* 35(4):666–669.

LÓPEZ-HONORATO, E., MEADOWS, P.J. & XIAO, P. 2009. Fluidized bed chemical vapor deposition of pyrolytic carbon – I. Effect of deposition conditions on microstructure. *Carbon*, 47(2):396–410. Available: ScienceDirect.

LÓPEZ-HONORATO, E., MEADOWS, P.J., XIAO, P., MARSH, G. & ABRAM, T.J. 2008. Structure and mechanical properties of pyrolytic carbon produced by fluidized bed chemical vapor deposition. *Nuclear Engineering and Design*, 238(11): 3121–3128. Available: ScienceDirect.

LUI, J., ZHANG, G., ZHOU, J., WANG, J., ZHAO, W. & CEN, K. 2009. Experimental study of acoustic agglomeration of coal-fired fly ash particles at low frequencies. *Powder Technology*, 193(1):20–25. Available at: ScienceDirect.

MURR, L.E. & SOTO, K.F. 2005. A TEM study of soot, carbon nanotubes, and related fullerene nanopolyhedra in common fuel-gas combustion sources. *Materials Characterization*, 55(1):50–65. Available at: ScienceDirect.

NICHOLS, G., BYARD, S., BLOXHAM, M.J., BOTTERILL, J., DAWSON, N.J., DENNIS A., DIART V., NORTH, N.C. & SHERWOOD, J.D. 2002. A review of the terms *Agglomerate* and *Aggregate* with a recommendation for nomenclature used in powder and particle characterization. *Journal of Pharmaceutical Sciences*, 91(10):2103–2109. Available at: InterScience.

NWU (North-West University). 2009. HTR fuel and materials. (Addendum obtained as part of a course attended on HTR Fuels and Materials). Potchefstroom. 26 p. (Unpublished.)

NOTHNAGEL, G. & VENTER, S. 2006. HTR fact book. (Addendum obtained as part of a course attended on HTR Fuels and Materials). Potchefstroom. 74 p. (Unpublished.)

ONISCHUK, A.A., DI STASIO, S., STRUNIN, V.P., KARASEV, V.V., BAKLANOV, A.M. & PANFILOV, V.N. 2000. Coulomb interaction during agglomeration process of soot aerosol nanoparticles. *Journal of Aerosol Science*, 31(Supplement 1):948–949. Available: ScienceDirect.

PUGMIRE, R.J., YAN, S., MA, M., SOLUM, M.S., JIANG, Y.J., EDDINGS, E.G. & SAROFIM, A.F. 2003. Soot formation process. Department of Chemical & Fuels Engineering Department of Chemistry University of Utah. http://www-acerc.byu.edu/News/Conference/2003/Presentations/Pugmire.pdf. Date of access 03 Mrt. 2010

QIAN, F. & WUB, Y. 2009. Effects of the inlet section angle on the separation performance of a cyclone. *Chemical Engineering Research and Design*. (In press). Available: ScienceDirect.

RAY, M.B., HOFFMANN, A.C. & POSTMA, R.S. 2000. Performance of different analytical methods in evaluating grade efficiency of centrifugal separators. *Journal of Aerosol Science*, 31(5):563–581. Available: ScienceDirect.

RAY, M.B., LUNING, P.E., HOFFMANN, A.C., PLOMP, A. & BEUMER, M.I.L. 1998. Improving the removal efficiency of industrial-scale cyclones for particles smaller than five micrometre. *International Journal of Mineral Processing,* 53(1–2):39–47. Available at: ScienceDirect.

SANTANA, J.D.A.M., ARNOSTI JR., S. & COURY, J.R. 2001. Performance of cylindrical-conical cyclones with different geometrical configurations. *Brazilian Journal of Chemical Engineering,* 18(3):1–13. Available at: SciELO.

SCIENCE DAILY. 2009. Dirty snow causes early runoff in Cascades, Rockies. ScienceDaily: 12 Jan. http://www.sciencedaily.com/releases/2009/01/090112093336.htm Date of access: 15 Oct. 2009.

SWANEY, C. 2007. Carnegie Mellon researchers urge regulators to rethink strategies for controlling soot emissions. http://www.cmu.edu/news/archive/2007/March/march1_soot.shtml Date of access: 15 Oct. 2009.

TSAI, P.-Y., SHIEH, H.-Y., LEE, W.-J. & LAI, S.-O. 2001. Health-risk assessment for workers exposed to polycyclic aromatic hydrocarbons (PAHs) in a carbon black manufacturing industry. *Science of the Total Environment*, 278(1–3):137–150. Available at: ScienceDirect.

UNER, C. 2007. HTR Fuel and materials. (Addendum obtained as part of a course attended on HTR Fuels and Materials). Potchefstroom. 20 p. (Unpublished.)

VANDER WAL, R.L. & TOMASEK, A.J. 2004. Soot nanostructure: dependence upon synthesis conditions. *Combustion and Flame*, 136(1–2):129–140. Available at: ScienceDirect.

WAN, G., SUN, G., XUE, X. & SHI, M. 2008. Solids concentration simulation of different size particles in a cyclone separator. *Powder Technology*, 183(1):94–104. Available: ScienceDirect.

WU, C.-Y., ALLEN, A., WINTZ, H., CHAPMAN, P., MARINI, J., YANG, S., ROBERG, R. & LI, Y. 2007. Learning about cyclones. Aerosol Science & Engineering: 12 Dec. http://aerosol.ees.ufl.edu/cyclone/section07.html Date of access: 14 Oct. 2009.

XIANG, R., PARK, S.H. & LEE, K.W. 2001. Effects of cone dimension on cyclone performance. *Journal of Aerosol Science*, 32(4):549–651. Available: ScienceDirect.

YANG, K.-S. & YOSHIDA, H. 2004. Effect of mist injection position on particle separation performance of cyclone scrubber. *Separation and Purification Technology*, 37(3):221–230. Available: ScienceDirect.

YOSHIDA, H., INADA, Y., FUKUI, K. & YAMAMOTO, T. 2009. Improvement of gas-cyclone performance by use of local fluid flow control method. *Powder Technology*, 193(1):6–14. Available: ScienceDirect.

ZHAO, B., SHEN, H. & KANG, Y. 2004. Development of a symmetrical spiral inlet to improve cyclone separator performance. *Powder Technology*, 145(1):47–50. Available: ScienceDirect.